



UNSW
S Y D N E Y

MMAN4951 – UG Thesis A

**An Investigation into the Height Effects of Vortex
Generators on Photovoltaic Module Temperature under
Forced Convection Conditions**

Interim Report and Project Plan

Author: Nathan Sivalingam, z5359644

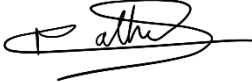
Supervisor: Dr Charitha de Silva

UNSW Sydney, School of Mechanical & Manufacturing Engineering

28/04/2025

Originality Statement

I, Nathan Sivalingam, hereby declare that this submission is my own work and to the best of my knowledge it contains no materials previously published or written by another person, or substantial proportions of material which have been accepted for the award of any other degree or diploma at UNSW or any other educational institution, except where due acknowledgement is made in the thesis. Any contribution made to the research by others, with whom I have worked at UNSW or elsewhere, is explicitly acknowledged in the thesis. I also declare that the intellectual content of this thesis is the product of my own work, except to the extent that assistance from others in the project's design and conception or in style, presentation and linguistic expression is acknowledged.

Signature: 

Date: 28th April 2025

Acknowledgements

I would like to express my sincere appreciation to Dr Charitha de Silva for the invaluable guidance provided throughout my thesis journey. The provision of resources, regular meetings, and continual support have been of immense benefit to my development as a student. I am deeply grateful for the time and effort dedicated to offering advice on the direction of my research, as well as for the trust placed in both myself and Shubhneet Sodhi as we progress into the experimental phase of this project. I look forward with great anticipation to the continuation of this project.

I would also like to express my gratitude to Matthew Deng, who has offered enormous support in both report writing and experimental preparation. Your knowledge and testing experience have been a significant help as I familiarised myself with the project. Furthermore, your commitment to the project is inspiring, and I am deeply appreciative of the time and effort you have dedicated to giving both myself and Shubhneet Sodhi the best opportunity for success. I am especially thankful for the warm welcome extended to me upon joining the project; your kindness has made me feel exceptionally fortunate.

I would also like to thank Shubhneet Sodhi for his support throughout the term. What once felt like a daunting task became a rewarding and enjoyable journey through the opportunity to work alongside someone who shares a similar passion. I look forward to continuing this work together, and perhaps, by the end, we will have earned the break.

Finally, I would like to thank my family and friends for their patience and support, whether it was listening to me speak aloud about boundary layers in the early hours of the morning or picking me up from the train station late at night. Any success I achieve, I owe to all of you.

Abstract

The growing demand for renewable energy sources has made the performance limitations of photovoltaic modules an increasingly prominent issue. In recent times, there has been increased attention paid to the decline in electrical efficiency experienced by photovoltaic modules at elevated temperatures. The already low electrical efficiency, typically ranging from 6% to 20%, is further reduced by the increased temperatures they experience during operation. The aims of this study were to conduct a comprehensive review of the existing methods used to reduce photovoltaic module temperature and to assess the most suitable method. Additionally, the study identified a gap in the literature concerning the effects of vortex generator height on photovoltaic module temperature under forced convection conditions. The results of this study lay the groundwork for experimental testing, which will enable a characterisation of the effect of vortex generator height on photovoltaic module temperature reduction.

Nomenclature

Parameters

Symbol	Definition	Unit
ϕ_0	Work function	J
K. E.	Kinetic energy of the emitted electron	J
h_p	Planck's constant	$6.626 \times 10^{-34} Js$
f_0	Threshold frequency	Hz
η	Electrical efficiency	-
V_{OC}	Open-circuit voltage	V
I_{SC}	Short circuit current	A
FF	Fill Factor	-
P_{in}	Input Power	W
J_0, I_0	Diode saturation current	A/m^2
q	Elementary charge	$1.602 \times 10^{-19} C$
k_b	Boltzmann's constant	$1.381 \times 10^{-23} J/K$
σ	Stefan-Boltzmann constant	$5.670 \times 10^{-8} W/m^2 K^4$
T	Temperature	K
E_G	Bandgap energy	eV
n	Ideality factor	-
I_L	Light generated current	A/m^2
J_{SC}	Short circuit current density	A/m^2
A	Cross-sectional area	m^2
v_{OC}	Normalised open-circuit voltage	-
\dot{Q}_{cond}	Rate of conductive heat transfer	J/s
k	Thermal conductivity	W/mK
ΔT	Temperature difference	K
Δx	Material thickness	m
\dot{Q}_{rad}	Rate of radiative heat transfer	J/s
ε	Emissivity of the surface	-

A_s	Surface area	m^2
T_s	Surface temperature	K
T_{surr}	Temperature of the surrounding environment	K
\dot{Q}_{conv}	Rate of convective heat transfer	J/s
h	Convective heat transfer coefficient	W/m^2K
T_∞	Temperature of the surrounding fluid	K
Ra_L	Rayleigh number	-
Ra_θ	Rayleigh number for an inclined plate	-
g	Acceleration due to gravity	$9.81 m/s^2$
β	Volumetric thermal expansion coefficient	$1/K$
L_C	Characteristic length	m
ν	Kinematic viscosity	m^2/s
α	Thermal diffusivity	m^2/s
θ	Angle of inclination	$^\circ$
Nu	Nusselt number	-
C	Constant dependent on geometry and flow conditions	-
m	Exponent dependent on geometry and flow conditions	-
u	Distance-specific fluid velocity	m/s
δ	Velocity boundary layer thickness	m
δ_t	Thermal boundary layer thickness	m
Re_D	Reynolds number of a cylinder	-
ρ	Fluid density	kg/m^3
V	Fluid velocity	m/s
D	Characteristic diameter	m
μ	Dynamic viscosity	$kg/m \cdot s$

Nu_{cyl}	Average Nusselt number for cross flow over a cylinder	-
Re	Reynolds number	-
Pr	Prandtl number	-
$E_{b\lambda}$	Spectral radiance of a blackbody	W/m^3
λ	Wavelength	μm
T_b	Absolute temperature of a blackbody	K
C_1	First radiation constant	$W \cdot \mu m^4/m^2$
C_2	Second radiation constant	$\mu m \cdot K$

Abbreviations

Abbreviation	Expansion
PV	Photovoltaic
MTFHS	Multidirectional Tapered Fin Heat Sinks
PCM	Phase Change Material
PDMS	Polydimethylsiloxane
NOCT	Nominal Operating Cell Temperature
VG	Vortex Generator
PIV	Particle Image Velocimetry
LWT	Large Wind Tunnel
IR	Infrared Camera
HSE	Health, Safety, and Environment
VH	Very High
H	High
M	Medium
L	Low

Contents

Originality Statement	i
Acknowledgements	ii
Abstract	iii
Nomenclature	iv
Parameters	iv
Abbreviations	vi
Table of Figures	ix
1. Introduction	1
2. Literature Review	2
2.1. Principles of Photovoltaic Modules	2
2.2. Performance Limitations of Photovoltaic Modules	3
2.3. Heat Transfer in Photovoltaic Modules	7
2.3.1. Conduction	8
2.3.2. Radiation	9
2.3.3. Convection	9
2.3.4. Vortex Generators	16
2.4. Experimental Techniques	19
2.4.1. Infrared Technology	19
2.4.2. Thermocouple Sensors	20
2.4.3. Particle Image Velocimetry	20
2.5. Literature Gap	21
3. Research Question and Project Plan	23
3.1. Experimental Methodology	23
3.2. Thesis Timeline	26
3.3. Available Resources Identified	28
3.4. Required training and upskilling identified	29
4. Project Dependent Preparations	30
4.1. Evidence of training on specific equipment	30
4.2. Evidence of some upskill in new software/methods	30

4.3.	Preliminary results (Aligned 75 mm VG Positioned on Roof).....	30
4.4.	Components/parts ordered	32
4.5.	Detailed budget of parts to be ordered	32
4.6.	Risk Assessment.....	33
5.	Conclusion	34
	References	35
	Appendix	A
	Appendix A: Thesis Timeline – Gantt Charts	A
	Appendix A.1: Term 1, 2025 Gantt Chart	A
	Appendix A.2: Term 1-2 Break, 2025 Gantt Chart	B
	Appendix A.3: Term 2, 2025 Gantt Chart	C
	Appendix A.4: Term 3, 2025 Gantt Chart	E
	Appendix B: Evidence of Training on Specific Equipment.....	F
	Appendix B.1: MME HSE Orientation session and Quiz.....	F
	Appendix B.2: Required Enrolment and Course Completion.....	G
	Appendix B.3: Induction into the Aerodynamics Lab	I
	Appendix C: Risk Assessment	J
	Appendix C.1: Identify Hazards and Control the Risks.....	J
	Appendix C.2: Risk Rating Matrix	M

Table of Figures

Figure 1: Photoelectric effect diagram. [70]	2
Figure 2: Photovoltaic Cell Structure Diagram. [14]	3
Figure 3: Electrical efficiency as a function of PV temperature. [7]	4
Figure 4: Diode saturation current as a function of band gap. The values are determined from detailed balance and place a limit on the open-circuit voltage of a solar cell. [22]	5
Figure 5: V_{OC} , as a function of band gap for a cell under AM 0 and AM 1.5 illumination. The V_{OC} increases with bandgap as the recombination falls. [22]	5
Figure 6: JSC as a function of band gap for a cell with AM 0 and AM 1.5. [23]	6
Figure 7: Fundamental Concept of heat transfer on a photovoltaic module. Adapted from [28]	7
Figure 8: The cooling of a boiled egg by natural convection. Adapted from [30]	9
Figure 9: Natural convective heat transfer on a horizontal plate. Adapted from [40]	10
Figure 10: Natural convective heat transfer on an inclined plate. Adapted from [40]	10
Figure 11: Inclined photovoltaic module. Adapted from [40]	11
Figure 12: The cooling of a boiled egg by forced convection. [30]	12
Figure 13: Velocity boundary layer over a flat plate. Adapted from [37]	12
Figure 14: Thermal boundary layer on a flat plate (the plate surface is hotter than the fluid). Adapted from [37]	13
Figure 15: Comparison of PV temperature when using air cooling over time. [44]	14
Figure 16: Comparison of efficiency when using air cooling over time. [44]	14
Figure 17: Comparison of PV temperature when using water sprinklers over time. [44]	14
Figure 18: Comparison of efficiency when water sprinklers over time. [44]	14
Figure 19: Comparison of PV temperature when using hybrid cooling over time. [44]	15
Figure 20: Comparison of efficiency when using hybrid cooling over time. [44]	15
Figure 21: Fluid flow over a cylinder. Adapted from [51]	16
Figure 22: Forward facing vortex generator arrangement. Adapted from [55]	18
Figure 23: Backward facing vortex generator arrangement. Adapted from [55]	18
Figure 24: Vortex Generator Geometry Configurations. Adapted from [56]	18
Figure 25: Spacing direction of vortex generator array relative to air direction of airflow. Adapted from [57]	19
Figure 26: Experimental arrangement for planar 2C-2D PIV in a wind tunnel. Adapted from [65]	21
Figure 27: 2D schematic illustration of the experimental setup inside and outside the LWT section. [57]	23
Figure 28: Isometric View of Experimental Rig	30

Figure 29: Front View of Experimental Rig	30
Figure 30: Side View of Experimental Rig.....	30
Figure 31: Thermal Image Capture and Corresponding Parameters (Cylinder_75_Roof_1ms1)	31
Figure 32: Term 1, 2025 Gantt Chart	A
Figure 33: Term 1-2 Break, 2025 Gantt Chart	B
Figure 34: Term 2, 2025 Gantt Chart	D
Figure 35: Term 3, 2025 Gantt Chart	E
Figure 36: Evidence of MME HSE Orientation session and Quiz Completion.....	F
Figure 37: Evidence of <i>Safety@UNSW</i> Course Completion.	G
Figure 38: Evidence of <i>Lab Health & Safety</i> Course Completion.....	H
Figure 39: Evidence of <i>Hazardous Chemicals</i> Course Completion.	H
Figure 40: Evidence of Aerodynamics Lab Induction.	I

1. Introduction

Throughout history, reliance on non-renewable energy sources has been central to the rapid advancement of human societies, ultimately culminating in the emergence of the modern world. Today, the global population, now exceeding eight billion, remains heavily dependent on these energy sources for survival and continued development. However, the accelerated pace of advancement, coupled with rapid population growth, has led to the exploitation of these finite resources, resulting in significant environmental damage and their depletion. Fossil fuels such as coal, oil, and natural gas are responsible for approximately 89% of global greenhouse gas emissions, which are recognised as the primary contributors to climate change. [1] Furthermore, the combustion of fossil fuels accounts for roughly 70% of global air pollution, a major factor in an estimated 7 million premature deaths annually worldwide. [2] Moreover, proven oil reserves are decreasing by 3-4% each year, as the rate of global extraction surpasses the discovery of new reserves, raising significant concerns about future supply shortages. [3]

To address this challenge, the large-scale development of renewable energy sources was initiated. Wind turbines harnessed wind energy, dams and rivers captured the power of flowing water, and photovoltaic modules converted solar energy into electricity. This marked a global shift in energy dependence, with populations transitioning from non-renewable to sustainable energy sources. As of 2024, renewable energy sources account for approximately 40.9% of global electricity generation, with solar power serving as the primary driver of this growth. [4]

As reliance on renewable energy sources grew, further investigation into their performance limitations became essential. One key issue identified was the reduction in the electrical efficiency of photovoltaic modules at elevated temperatures. In their seminal 1961 paper, *Detailed Balance Limit of Efficiency of p-n Junction Solar Cells*, William Shockley and Hans Queisser established the theoretical maximum efficiency of silicon-based solar cells at approximately 30% under standard illumination conditions. [5] Moreover, the electrical efficiency of a typical photovoltaic module generally ranges from 6% to 20%. [6] In 2010, H.G. Teo observed the inverse relationship between the electrical efficiency of photovoltaic modules and their operating temperature, noting that higher temperatures result in further efficiency losses. [7] Specifically, for every degree Celsius above the optimal temperature of 25°C, the electrical efficiency decreases by 0.5%. [8]

Therefore, this thesis intends to explore methods designed to reduce the elevated temperatures of photovoltaic modules. These methods will be assessed based on their effectiveness in lowering module temperature and, consequently, enhancing electrical efficiency. Through a thorough investigation and evaluation of these approaches, the thesis plans to identify the most promising cooling method for further study.

2. Literature Review

2.1. Principles of Photovoltaic Modules

Photovoltaic (PV) modules, also known as solar panels, are devices that convert sunlight into electrical energy. [9], [10]

Sunlight is made up of massless particles called photons, which possess a certain amount of energy. When these photons strike a surface, they knock electrons off the surface, known as photoelectrons. This is known as the photoelectric effect, shown in Figure 1.

The photoelectric effect will occur only if the frequency of the radiation is greater than the threshold frequency of the metal. The threshold frequency is the minimum frequency of light that causes electrons to be emitted from a material. The proportional relationship that exists between the threshold frequency, f_0 , and the work function, ϕ_0 , is shown in Equation 1.

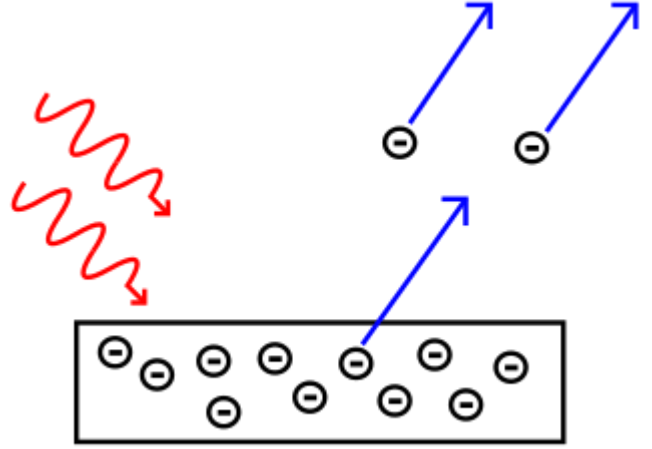


Figure 1: Photoelectric effect diagram. [70]

$$h_p f_0 = \phi_0 + \text{K. E.} \quad (1)$$

The work function refers to the minimum amount of energy needed to remove an electron from a metal surface. If photons with enough energy hit the surface, they can transfer their energy to the electrons allowing them to escape. If the energy of the incident photons is less than the work function, no electrons will be emitted, regardless of the light's intensity. [11]

A photovoltaic module is made up of multiple photovoltaic cells, commonly known as solar cells. Each photovoltaic cell is made of semiconductor material, which is placed between the conductive layers. The most common semiconductor material used to make photovoltaic cells is silicon, accounting for 95% of photovoltaic modules sold worldwide. [12] These photovoltaic cells use the photoelectric effect to convert solar energy into electrical energy.

As shown in Figure 2, a silicon photovoltaic cell is composed of two different layers of silicon: an n-type silicon layer, which has additional electrons, and a p-type silicon layer, which has extra spaces for the electrons, called holes.

Both the n-type and p-type silicon layers undergo a process known as doping; whereby specific impurities are intentionally introduced into an intrinsic semiconductor to enhance its electrical conductivity. The n-type silicon layer is doped with atoms such as arsenic or phosphorus, which possess one more valence electron than silicon atoms, thereby introducing additional free electrons into the material. Consequently, the n-type layer becomes negatively charged. Conversely, the p-type silicon layer is doped with elements

such as boron or gallium, which possess one fewer valence electron than silicon atoms, creating electron deficiencies known as holes. As a result, the p-type layer acquires a positive charge. At the interface between the n-type and p-type layers, surplus electrons from the n-type region migrate to fill the holes in the p-type region, establishing an electric field across the p–n junction. This region is referred to as the depletion zone. [13]

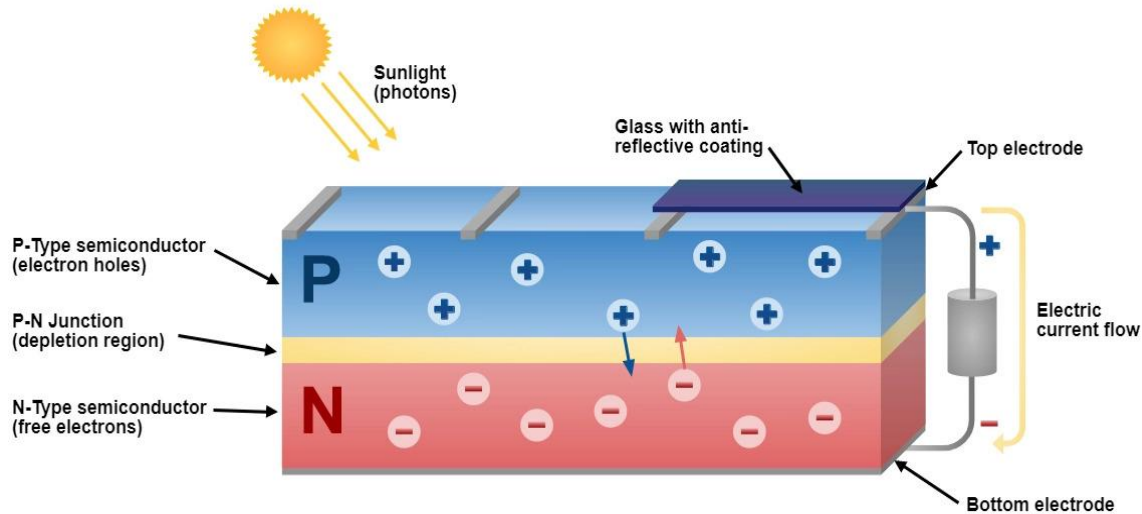


Figure 2: Photovoltaic Cell Structure Diagram. [14]

When a photon strikes the silicon photovoltaic cell with the required energy, an electron is knocked out of its bond. Because of the electric field at the p-n junction, the negatively charged electron moves toward the n-side, while the resulting positively charged hole is attracted to the p-side. The free electrons are collected by thin metal fingers positioned at the top of the photovoltaic cell, before travelling through an external circuit. After electrical work is performed, the electrons are returned to the conductive aluminium sheet positioned at the back of the photovoltaic cell. Since electrons follow a continuous cycle and are the only moving components, there is no wear and tear, allowing photovoltaic cells to last for decades. [15] However, they still have limitations.

2.2. Performance Limitations of Photovoltaic Modules

A major limitation of photovoltaic modules is their declining electrical efficiency, particularly at high temperatures.

A review led by Swapnil Dubey of Nanyang Technological University found that standard photovoltaic modules typically convert 6-20% of incoming solar radiation into electrical energy. The remaining 80-94% is mostly converted into heat, increasing the module's temperature and further lowering its efficiency. [6]

A 2010 study led by H.G. Teo from the National University of Singapore refined Dubey et al.'s electrical efficiency range to 8-14%. In the study, Teo et al. focused on comparing the electrical efficiency of photovoltaic modules under cooling and non-cooling conditions. Teo et al. observed that the electrical

efficiency of the photovoltaic module decreased as the temperature of the module increased, as shown in Figure 3. Teo et al. also found that without active cooling, the module temperature was significantly higher than when active cooling was applied under the same meteorological conditions. Thus, active cooling improved the module's electrical efficiency from 8–9% to 12–14%. [7]

The inverse linear relationship between the temperature and the electrical efficiency of a photovoltaic module is attributed to the band gap reduction, which occurs as the module's temperature increases.

In 1931, A.H. Wilson's paper, *The Theory of Electronic Semi-Conductors*, introduced the idea that semiconductors have a small but finite band gap that affects their electrical conductivity. [16]

The band gap represents the amount of energy that an electron must possess to jump from the valence band, where valence electrons are confined, to the conduction band. When valence electrons receive enough energy from an external source, they can undergo this band transition, which allows the material to conduct electricity. [17] As the temperature of the photovoltaic module increases, the valence electrons in the semiconductor material are excited. Thus, the energy required for an electron to transition from the valence band to the conduction band decreases, as indicated by a reduction in the band gap. [18]

To understand the proportional relationship between the band gap and the electrical efficiency, an inspection of the formula used to calculate the electrical efficiency of a photovoltaic cell, shown in Equation 2, is required. [19]

$$\eta = \frac{V_{OC} I_{SC} FF}{P_{in}} \quad (2)$$

The open circuit voltage, V_{OC} , short circuit current, I_{SC} , and fill factor, FF , are all affected by the band gap. Therefore, an investigation into the effect of a reduced band gap on these variables is necessary to evaluate the impact that the band gap has on the electrical efficiency of the photovoltaic module.

A 1994 study led by P. Baruch from the University of Paris derived a formula for determining the minimum value of the diode saturation current, as shown in Equation 3. [20]

$$J_0 = \frac{q}{k} \frac{15\sigma}{\pi^4} T^3 \int_{\frac{E_G}{k_b T}}^{\infty} \frac{x^2}{e^x - 1} dx \quad (3)$$

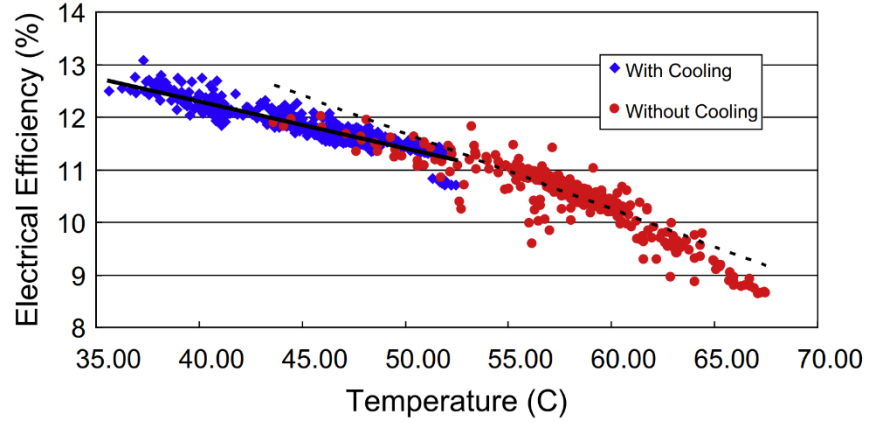


Figure 3: Electrical efficiency as a function of PV temperature. [7]

A casual inspection of Equation 3 reveals a relationship between the band gap energy, E_G , and the diode saturation current, J_0 . However, it is not immediately obvious what the nature of the relationship is due to the complexity of the integral function.

Just over a decade later, Michael Y. Levy and Christiana Honsberg from the University of Delaware proposed a method to evaluate the integral in Baruch's formula. [21] Then, in 2017, Honsberg worked with Stuart Bowden to graph the relationship between the diode saturation current and the band gap based on this method, as shown in Figure 4. Honsberg and Bowden used the diode saturation current values, J_0 , from Figure 4, denoted as I_0 in Equation 4, to calculate the open-circuit voltage, V_{OC} , as a function of the band gap. The linear proportional relationship between the band gap and the open-circuit voltage is shown in Figure 5.

$$V_{OC} = \frac{nk_bT}{q} \times \ln\left(\frac{I_L}{I_0} + 1\right) \quad (4)$$

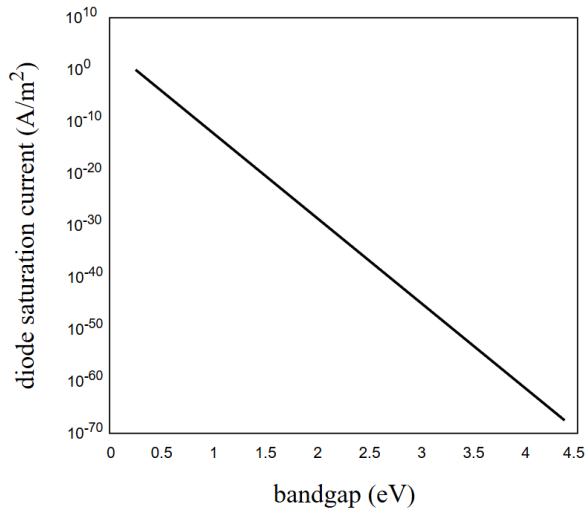


Figure 4: Diode saturation current as a function of band gap. The values are determined from detailed balance and place a limit on the open-circuit voltage of a solar cell. [22]

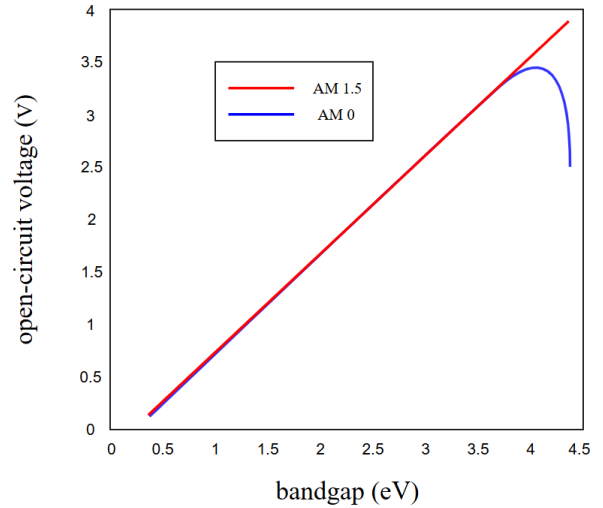


Figure 5: V_{OC} , as a function of band gap for a cell under AM 0 and AM 1.5 illumination. The V_{OC} increases with bandgap as the recombination falls. [22]

Thus, the reduced band gap due to the increased temperature of the photovoltaic module leads to a decrease in the open-circuit voltage. [22]

Honsberg and Bowden also graphed the relationship between the band gap and the short-circuit current density, as shown in Figure 6. From Figure 6, it is evident that a band gap reduction corresponds to an increase in the short-circuit current density. Equation 5 shows a linearly proportional relationship between the short-circuit current and the short-circuit current density.

$$I_{SC} = J_{SC}A \quad (5)$$

Therefore, a decrease in the band gap leads to an increase in the short-circuit current. [23]

In 1981, M.A. Green of the University of New South Wales proposed an empirical expression for the fill factor, as shown in Equation 6.

As established earlier in Figure 5, a band gap reduction corresponds to a decrease in the open-circuit voltage. An evaluation of Equation 6 reveals that a decline in the open-circuit voltage, V_{OC} , and an increase in the temperature of the photovoltaic module, T , causes a decrease in the fill factor, FF . Therefore, it can be concluded that a band gap reduction causes a decrease in the fill factor.

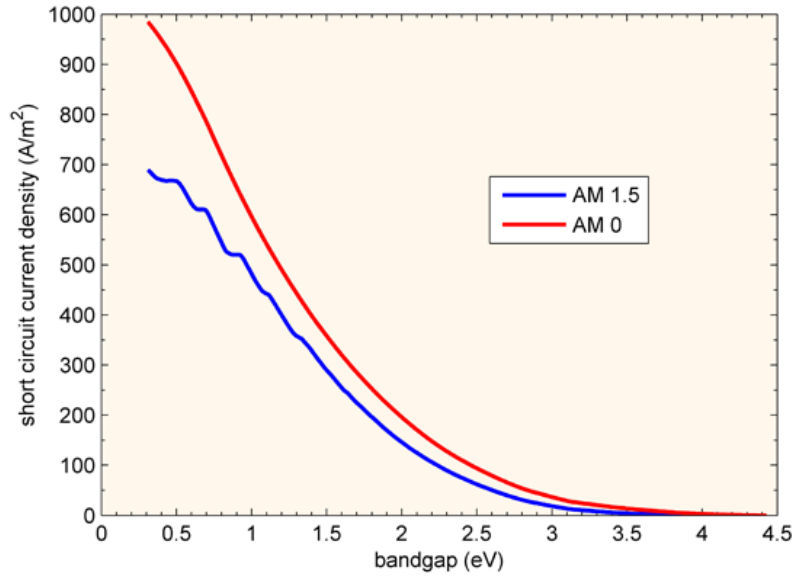


Figure 6: J_{SC} as a function of band gap for a cell with AM 0 and AM 1.5. [23]

$$FF = \frac{v_{OC} - \ln(v_{OC} + 0.72)}{v_{OC} + 1} \quad (6)$$

Where v_{OC} is defined as a normalised V_{OC} : $v_{OC} = \frac{q}{nk_b T} V_{OC}$. [24]

To summarise, the band gap reduction that arises due to the increased temperature of the photovoltaic module causes a decrease in the open-circuit voltage, an increase in the short circuit current and a decrease in the fill factor. While the short circuit current does increase, it is ultimately outweighed by the decrease in the open-circuit voltage and fill factor, leading to a decrease in the module's electrical efficiency.

In addition to temperature, other environmental factors like shade and air pollution limit the electrical efficiency of photovoltaic modules. A 2013 study led by Alberto Dolara from the Polytechnic University of Milan found that shade significantly affects the performance of photovoltaic modules. Dolara et al. observed a 31% drop in the power generated by a single photovoltaic cell when 50% of the cell was subjected to shade. [25] In 2001, E. Asl-Soleimani et al. from the University of Tehran concluded that air pollution also reduced the energy output of photovoltaic modules by up to 60%. [26] Furthermore, operational factors like poor module maintenance can lead to dust buildup, significantly reducing power generation. A review led by Khaled Hasan in 2021 stated a 60-70% reduction in power generation due to the deposition of dust in humid conditions. [27]

In 1961, William Shockley and Hans Queisser published their paper, *Detailed Balance Limit of Efficiency of p-n Junction Solar Cells*, in which they established the theoretical maximum efficiency of silicon-based solar cells to be approximately 30% under standard illumination conditions. [5] However, in the real world, photovoltaic cells are prevented from reaching this limit due to the environmental and operational factors previously discussed. Thus, due to the important role that photovoltaic modules play in the future of global energy, methods to reduce the impact that these factors have on the performance of photovoltaic modules are constantly being investigated. To mitigate the reduction in electrical efficiency caused by increased photovoltaic module temperature, heat transfer-based cooling methods are investigated and employed worldwide.

2.3. Heat Transfer in Photovoltaic Modules

The fundamental concept of heat transfer is the process by which heat energy moves from one system or body to another because of a temperature difference. This transfer of heat can occur via conduction, convection or radiation. Figure 7 demonstrates the fundamental concept of heat transfer in the context of a photovoltaic module.

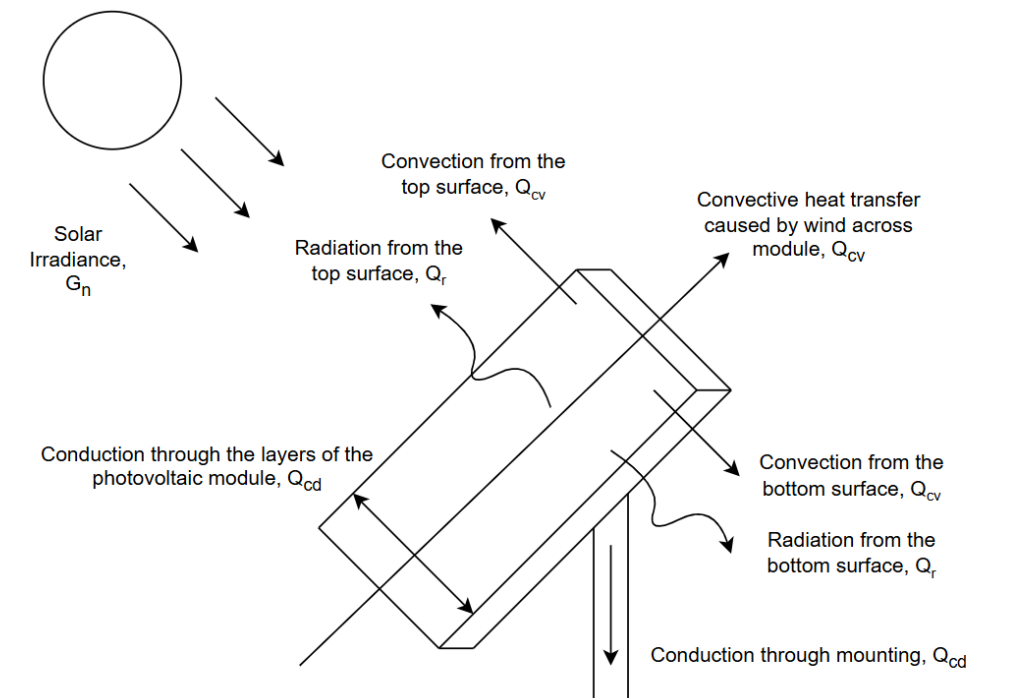


Figure 7: Fundamental Concept of heat transfer on a photovoltaic module. Adapted from [28]

In Figure 7, conductive heat transfer through the layers of the photovoltaic module and the mounting are observed. Additionally, heat is transferred from the surface of the photovoltaic module to the surrounding air via convection. Finally, the module emits thermal radiation to its surroundings, contributing to radiative heat transfer. In 2020, P. Dwivedi from the Maulana Azad National Institute of Technology, Bhopal, analysed the percentage distribution of heat loss across the different modes of heat transfer, shown in Table 1. [29]

Table 1: Heat loss from photovoltaic module. [29]

S. No	Heat loss from module	Percentage
1	Conduction from the mounting	2
2	Convection from the top surface	42
3	Convection from the bottom surface	24
4	Radiation from the top surface	21
5	Radiation from the bottom surface	5

An inspection of Table 1 reveals that convection is the dominant mode of heat transfer in photovoltaic modules. Consequently, a given percentage increase in the rate of convective heat transfer will have a greater impact on the overall module heat dissipation than an equivalent increase in conductive or radiative heat transfer. Therefore, the following subsections will examine the effectiveness of conduction-, convection-, and radiation-based cooling methods in reducing photovoltaic module temperatures to enhance overall efficiency, with particular emphasis on convection-based approaches.

2.3.1. Conduction

Conduction is the transfer of energy from the more energetic particles of a substance to the adjacent less energetic ones because of interactions between the particles. The formula commonly used to calculate the rate of heat conduction is shown in Equation 7. [30]

$$\dot{Q}_{\text{cond}} = -kA \frac{\Delta T}{\Delta x} \quad (7)$$

The main conduction-based cooling methods used to reduce photovoltaic module temperatures are finned heat sinks and phase change materials.

A heat sink is a component used in thermal management strategies to transfer heat effectively. Its design is optimised to dissipate heat. [31] The use of a heat sink increases the cross-sectional area that the heat is being transferred to, denoted as A in Equation 7. Through further inspection of Equation 7, it is observed that the increased cross-sectional area, A , results in an increased rate of conductive heat transfer, \dot{Q}_{cond} . A study led by S.N. Razali from the National University of Malaysia investigated the effect of multidirectional tapered fin heat sinks (MTFHS) on photovoltaic modules. Razali et al. found that the proposed MTFHS reduced the module's temperature by 12°C, indicating enhanced conductive heat transfer, which consequently improved the photovoltaic module's efficiency by 1.53%. [32]

A phase change material (PCM) is a material that can change its state from solid to liquid and vice versa by releasing and storing thermal energy. [33] When the surrounding temperature rises above the PCM's melting point, it liquefies, drawing heat away from the photovoltaic module. Conversely, when the temperature drops below the melting point, the PCM solidifies, releasing the stored heat back into the environment. A 2023 study by B. Hussain and colleagues at the Capital University of Science &

Technology found that incorporating PCM lowered the surface temperature of photovoltaic modules by 13.1°C, resulting in a 6.85% increase in efficiency. [34]

2.3.2. Radiation

Radiation is the energy emitted by matter in the form of electromagnetic waves (or photons) due to changes in the electronic configurations of the atoms or molecules. In the context of heat transfer, the focus is on thermal radiation, which is the energy emitted by bodies due to their temperature. The formula commonly used to calculate the rate of radiation heat transfer is shown in Equation 8. [30]

$$\dot{Q}_{\text{rad}} = \varepsilon \sigma A_s (T_s^4 - T_{\text{surr}}^4) \quad (8)$$

In 2018, a study led by B. Zhao from the University of Science and Technology of China investigated the performance impact of radiation-based cooling methods on photovoltaic modules. Zhao et al. modified a photovoltaic module by adding a polydimethylsiloxane (PDMS) film on its top surface. PDMS is known to have high emissivity in the mid-infrared range (8 – 13 μm). [35] Through an inspection of Equation 8, it is observed that an increased emissivity, ε , causes an increase in the rate of radiative heat transfer, \dot{Q}_{rad} . In theory, the increased radiative heat transfer of the photovoltaic module lowers the module's temperature and improves its efficiency. However, Zhao et al. found that the temperature of the photovoltaic module was only reduced by 1.75 K in the ideal case. Furthermore, this result was achieved using a simulated environment. Thus, Zhao's team concluded that, in practical applications, enhanced radiative cooling does not offer significant potential for cooling photovoltaic modules. [36]

2.3.3. Convection

Convection is the mode of energy transfer between a solid surface and the adjacent liquid or gas that is in motion. The formula commonly used to calculate the rate of convective heat transfer can be expressed by Newton's law of cooling, shown in Equation 9. [30]

$$\dot{Q}_{\text{conv}} = h A_s (T_s - T_{\infty}) \quad (9)$$

Convection is not a fundamental heat transfer mechanism; rather, it is a combined phenomenon, where heat conduction occurs in the presence of fluid motion. Convection can be broadly categorised into two types: natural convection, also referred to as free convection, and forced convection. [37]

2.3.3.1. Natural Convection and Relevant Cooling Methods

Natural Convection is the process by which heat transferred to a fluid raises its temperature, reducing its density and generating buoyant forces. These forces cause the warmer, lighter fluid to rise, carrying the absorbed heat to another location where it can be dissipated. [38] Figure 8 illustrates natural convective heat transfer in the context of cooling a hot egg.

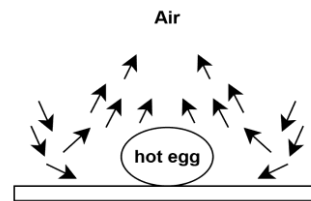


Figure 8: The cooling of a boiled egg by natural convection. Adapted from [30]

2.3.3.1.1. Tilt Angle Optimisation

The tilt angle of a photovoltaic module significantly influences natural convective heat transfer, as it alters the buoyancy-driven airflow around the module's surface.

A 2021 study led by A. Abdulmunem from the University of Malaya, Malaysia, investigated the impact of tilt angle on the performance of photovoltaic systems. Abdulmunem et al. observed that as the tilt angle increased from 0° (horizontal) to 90° (vertical), the temperature reduction in the photovoltaic cell increased from -0.4% to -12% . This trend was attributed to enhanced natural convective heat transfer which acts to improve photovoltaic module efficiency. Consequently, Abdulmunem et al. concluded that increasing the tilt angle of the photovoltaic module away from the horizontal axis and towards the vertical axis improves the rate of convective heat transfer. [39]

2.3.3.1.2. Natural Convection Boundary Layers

To understand the effect of the tilt angle on natural convective heat transfer, it is necessary to first understand the velocity and thermal boundary layers. The velocity boundary layer describes how the fluid's motion adjusts from being stationary at the surface to moving freely away, while the thermal boundary layer describes how heat diffuses into or from the fluid at the surface. The thermal and velocity boundary layers are interconnected, with fluid motion influencing heat transfer, and their relative thickness depends on the fluid's properties. The relationship between the thermal and velocity boundary layers is characterised by the Prandtl number, Pr . A more in-depth breakdown of boundary layers can be found in **Section 2.3.3.2**.

As shown in Figure 9, at lower tilt angles (near horizontal), the heated air tends to remain attached to the surface for a longer duration, as the buoyancy forces are predominantly vertical. This results in the formation of a thicker and more stable thermal boundary layer, which promotes relatively weak convection. In contrast, as shown in Figure 10, when the surface aligns more closely with the direction of the buoyant forces, the hot air can rise more freely along the surface. This facilitates a thinner thermal boundary layer and an increased air velocity near the surface, thereby enhancing convective heat transfer.

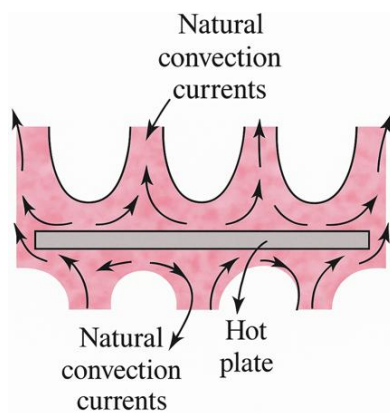


Figure 9: Natural convective heat transfer on a horizontal plate. Adapted from [40]

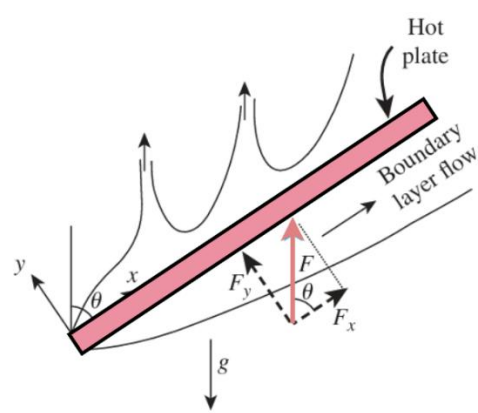


Figure 10: Natural convective heat transfer on an inclined plate. Adapted from [40]

2.3.3.1.3. Tilt Angle Optimisation: A Theoretical Confirmation

Abdulmunem's conclusion is also in excellent agreement with the theoretical relationship between the photovoltaic module's tilt angle and the natural convective heat transfer rate. The Rayleigh number, Ra_L , which can be calculated using Equation 10, is the ratio of buoyancy forces and (the products of) thermal and momentum diffusivities. [40]

$$Ra_L = \frac{g\beta(T_s - T_\infty)L_c^3}{\nu\alpha} \quad (10)$$

For an inclined photovoltaic module between 0° and 60° , the gravitational force, g , is replaced with $g \sin(\theta)$, where θ represents the tilt angle between the horizontal axis and the photovoltaic module, shown in Figure 11.

Thus, Equation 11 is the appropriate mathematical expression for the Rayleigh number of a tilted photovoltaic module, Ra_θ . [40]

$$Ra_\theta = \frac{g \sin(\theta) \beta(T_s - T_\infty)L_c^3}{\nu\alpha} \quad (11)$$

A casual inspection of Equation 11 indicates that the Rayleigh number for a tilted photovoltaic module, Ra_θ , is directly proportional to the tilt angle, θ , within the range of 0° to 60° . [40] Therefore, increasing the tilt angle within this range results in a corresponding increase in the Rayleigh number.

The Nusselt number, Nu , is the ratio of convective to conductive heat transfer. [41] For simple empirical correlations in natural convection, an exponential relationship exists between the average Nusselt number, Nu , and the relevant Rayleigh number, shown in Equation 12. [40]

$$Nu = C Ra_\theta^m \quad (12)$$

Therefore, the increase in the Rayleigh number leads to an increase in the Nusselt number. Moreover, Equation 13 reveals that an increase in the Nusselt number, Nu , causes an increase in the convective heat transfer coefficient, h . [40]

$$h = \frac{Nu \times k}{L_c} \quad (13)$$

Finally, an inspection of Equation 9 reveals that an increase in the convective heat transfer coefficient, h , results in a higher convective heat transfer rate, \dot{Q}_{conv} , thereby supporting Abdulmunem et al.'s experimental findings. [30]

While a vertical photovoltaic module improves natural convective heat transfer, it limits the surface area that is directly exposed to the sun, reducing power output. Thus, a tilt angle of 45° from the horizontal

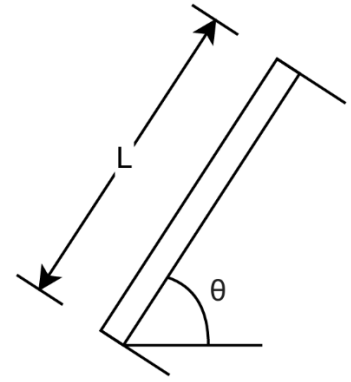


Figure 11: Inclined photovoltaic module.
Adapted from [40]

axis (as in earlier NOCT testing [42]) is generally used in photovoltaic module testing because it represents more realistic conditions.

2.3.3.1.4. Comparing the Effects of Natural Convection and Forced Convection on Photovoltaic Module Temperature Reduction

Natural convection-based cooling methods can effectively reduce an object's temperature; however, in photovoltaic modules, forced convection is significantly more efficient at transferring heat to the surroundings, resulting in greater improvements in module efficiency. A 2021 study led by A. Almuwailhi from King Saud University investigated the impact of both natural and forced convection cooling methods on the efficiency of photovoltaic modules. To promote natural convective heat transfer, Almuwailhi's team experimented with various channel air gaps. The most promising configuration featured an air gap height of 120 mm, which led to a 1.2% increase in photovoltaic module efficiency. For forced convection, Almuwailhi's team used airflow velocities of 2 m/s and 3 m/s. The results revealed a 3.8% increase in efficiency with 2 m/s airflow, and a 4% increase with 3 m/s airflow. [43] As a result, the remainder of this literature review will be dedicated to a comprehensive examination of forced convection cooling methods.

2.3.3.2. Forced Convection and Relevant Cooling Methods

Forced convection is a mode of heat transfer in which fluid flow over a surface is induced by external means such as a fan, pump, or wind, rather than resulting from natural buoyancy forces. [30] Figure 12 illustrates how forced convective heat transfer can be applied to cool a hot egg.

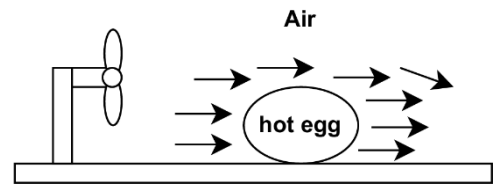


Figure 12: The cooling of a boiled egg by forced convection. [30]

Like natural convection, forced convection involves the development of velocity and thermal boundary layers that control momentum and heat transfer in the vicinity of the surface.

2.3.3.2.1. Forced Convection Boundary Layers

Figure 13 illustrates the velocity profile caused by parallel fluid flow over a flat plate. To understand this velocity profile, the fluid is modelled as a series of adjacent layers stacked on top of one another. The fluid particles in the layer closest to a solid surface are subject to the no-slip condition, which states that their velocity must match that of the boundary, resulting in zero relative motion between the fluid and the surface. Since photovoltaic modules remain stationary during operation, the fluid layer in direct contact with the surface has a velocity, $u = 0$.

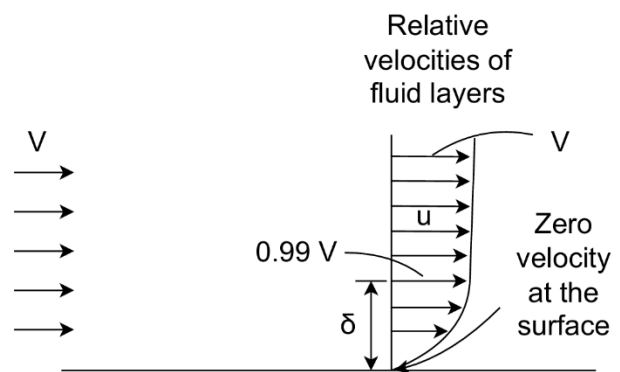


Figure 13: Velocity boundary layer over a flat plate. Adapted from [37]

The stationary fluid layer adjacent to the surface exerts frictional resistance on the fluid layer above it, reducing its velocity through shear interaction between layers moving at different speeds. This process propagates through successive fluid layers, each experiencing a reduction in momentum due to shear from the layer beneath, resulting in a velocity profile that increases with distance from the surface, but at a decreasing rate. At the boundary layer thickness, δ , the plate has negligible effect on the velocity of the fluid. Thus, δ , is typically defined as the distance from the surface where $u = 0.99V$. Therefore, the velocity boundary layer can be defined as the region of flow above the plate, bounded by δ , where the effects of viscous shearing forces are significant. [37]

Figure 14 shows the temperature profile that results due to the flow of parallel fluid over a flat plate. Given the focus on reducing photovoltaic module temperature, it is appropriate to illustrate a thermal boundary layer diagram where the plate surface is at a higher temperature than the surrounding fluid.

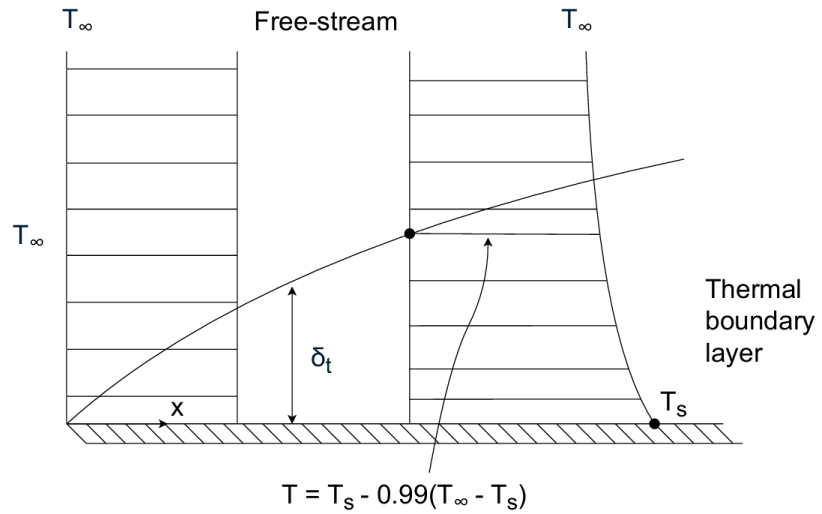


Figure 14: Thermal boundary layer on a flat plate (the plate surface is hotter than the fluid). Adapted from [37]

The fluid particles adjacent to the surface of the plate reach thermal equilibrium with the plate, adopting a temperature, T_s . This fluid layer transfers energy to the layer directly above it, resulting in a temperature gradient where each successive layer has a slightly lower temperature than the previous one, with the rate of decrease diminishing progressively. The boundary layer thickness, δ_t , represents the perpendicular distance from the flat plate at which the influence of the plate's temperature, T_s , on the fluid temperature, T_∞ , becomes negligible. Thus, the thickness of the thermal boundary layer at any location on the surface occurs when $T = T_s - 0.99(T_s - T_\infty)$. Therefore, the thermal boundary layer is defined as the flow region above the surface, bounded by δ_t , where the temperature variation in the direction normal to the surface is significant. [37]

A thicker thermal boundary layer results in a more gradual temperature gradient at the surface, reducing the effectiveness of convective cooling. To overcome this limitation, forced convection techniques are employed to disrupt and thin the boundary layer, enhancing the temperature gradient at the surface. This increase in the gradient leads to a higher convective heat transfer rate, which lowers the operating temperature of the photovoltaic module and subsequently improves its efficiency.

2.3.3.2.2. Air-Based Cooling Methods

In 2024, a study led by I. Al-Masalha from Al-Balqa Applied University investigated the enhancement of photovoltaic module efficiency through various cooling techniques, including air fans, water

sprinklers, and hybrid systems. One of the approaches involved directing airflow over the surface of the modules using air fans. This method resulted in a module temperature reduction ranging from 6% to 26%, as shown in Figure 15. Correspondingly, this temperature decrease led to an improvement in electrical efficiency within the range of 0.44% and 1.45%, as illustrated in Figure 16. [44]

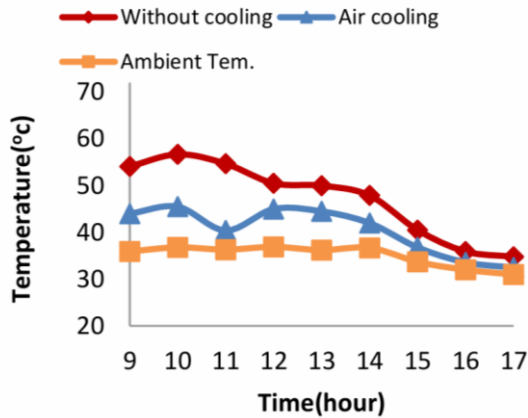


Figure 15: Comparison of PV temperature when using air cooling over time. [44]

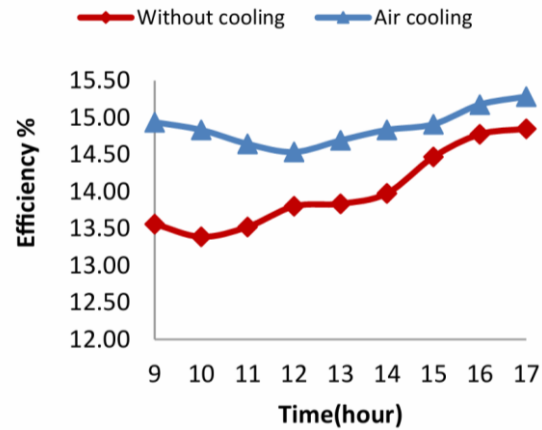


Figure 16: Comparison of efficiency when using air cooling over time. [44]

2.3.3.2.3. Water-Based Cooling Methods

Al-Masalha et al.'s water cooling method involved spraying water directly onto the photovoltaic modules to dissipate heat. As illustrated in Figure 17, this technique resulted in a temperature reduction of the photovoltaic module ranging from 20.45% to 35.44%. Consequently, as shown in Figure 18, this temperature reduction led to an efficiency improvement between 0.6% and 1.8%. [44]

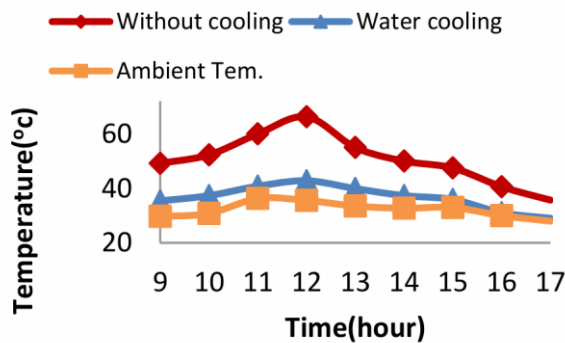


Figure 17: Comparison of PV temperature when using water sprinklers over time. [44]

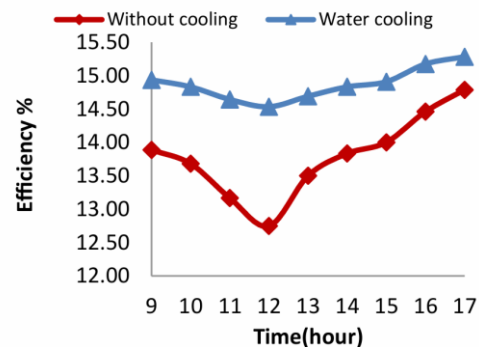


Figure 18: Comparison of efficiency when using water sprinklers over time. [44]

2.3.3.2.4. Hybrid Cooling Methods

In their final approach, Al-Masalha's team developed a hybrid cooling system by combining water spraying and air-cooling techniques. This integrated method produced the most significant results in terms of both temperature reduction and efficiency improvement. The hybrid cooling system achieved a temperature reduction in the range of 30% and 40%, shown in Figure 19. This substantial reduction in

temperature led to an increase in photovoltaic module efficiency, ranging from 0.88% to 2%, as illustrated in Figure 20. [44]

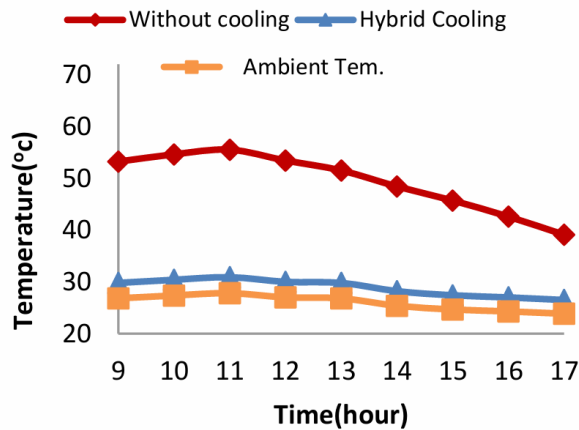


Figure 19: Comparison of PV temperature when using hybrid cooling over time. [44]

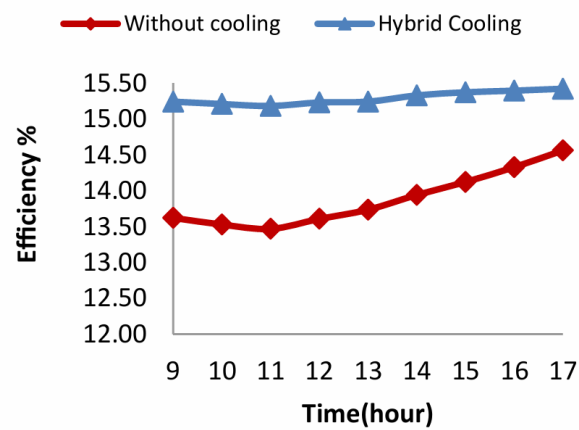


Figure 20: Comparison of efficiency when using hybrid cooling over time. [44]

2.3.3.2.5. Nanofluid-Based Cooling Methods

In recent times, nanofluid-based cooling methods have emerged as a highly effective technique for enhancing the thermal management and overall efficiency of photovoltaic modules. In 2022, T.K. Murtadha et al. conducted an experimental investigation into the performance enhancement of photovoltaic modules using titanium dioxide nanofluids. Their findings indicated that higher nanoparticle concentrations correlated with improved heat dissipation, resulting in a maximum efficiency gain of 19.23% under optimal nanofluid cooling conditions. [45]

2.3.3.2.6. An Assessment and Conclusion on the Most Promising Cooling Method

The studies conducted by Al-Masalha et al. [44] and Murtadha et al. [45] clearly demonstrate that water and nanofluid cooling methods outperform air-based cooling in terms of thermal regulation and efficiency improvement for photovoltaic modules. However, despite their superior performance, water and nanofluid cooling systems are significantly less prevalent than air cooling in photovoltaic applications. This disparity is primarily due to several practical limitations. Both water and nanofluid systems entail higher initial and operational costs, as well as increased system complexity. [29], [46] Additionally, they demand more frequent and intensive maintenance compared to air cooling systems, further escalating long-term expenses. [47], [48] Moreover, the structural load associated with liquid-based cooling is greater due to the added weight of the coolant medium, which imposes additional design and material constraints. [49] These factors collectively impact the cost-effectiveness of photovoltaic cooling strategies, rendering air cooling the most viable option for both commercial and residential implementations. Consequently, air cooling remains the most employed method for photovoltaic module thermal management. [29]

As was stated previously, Al-Masalha et al. implemented active cooling of photovoltaic modules using electric powered air fans to facilitate convective heat transfer. [44] However, this approach incurs a

parasitic energy cost, as external power is required to operate the fans. Vortex generators provide a passive cooling alternative that uses wind to induce localised turbulence and enhance convective heat transfer. Therefore, this literature review will examine the application of vortex generators in enhancing the thermal management of photovoltaic modules, ultimately leading to improved module efficiency.

2.3.4. Vortex Generators

Vortex generators are protrusions on a heat transfer surface that induce swirling flow around an axis, generating vortices that enhance convective heat transfer. [50] Figure 21 illustrates this phenomenon for a cylindrical vortex generator interacting with the surrounding fluid.

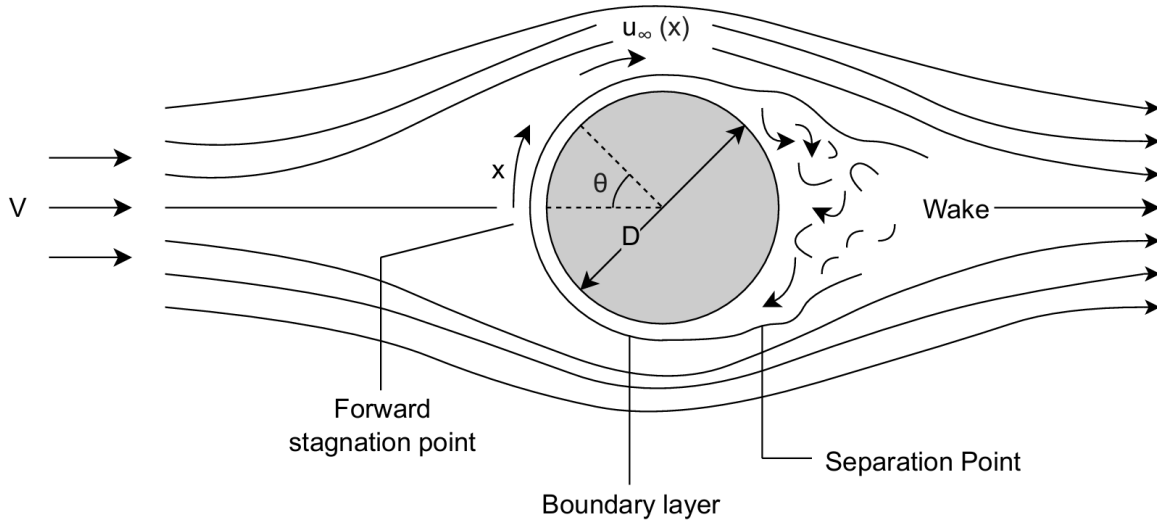


Figure 21: Fluid flow over a cylinder. Adapted from [51]

Figure 21 also draws attention to two key features associated with vortex generators: the forward stagnation point and the separation point. At the forward stagnation point, the fluid velocity, u , is zero, while the separation point marks the location where the airflow detaches from the surface of the object. At the separation point, vortices, referred to as Kármán vortices in the context of cylindrical bodies, are generated. [52] These vortices promote mixing between the high-momentum outer fluid and the low-momentum near-wall fluid, enhancing momentum and energy exchange near the surface. This mixing leads to the thinning of the thermal boundary layer. As discussed in **Section 2.3.3.2.1**, an inverse relationship exists between the thermal boundary layer thickness and the rate of convective heat transfer. Therefore, the reduction in boundary layer thickness results in an enhanced convective heat transfer rate.

2.3.4.1. Vortex Generators: A Theoretical Confirmation

The location of the separation point on a cylinder depends on the boundary layer's transition from laminar to turbulent flow. This transition is primarily characterised by the Reynolds number, Re_D , defined as the ratio of inertial to viscous forces in the fluid. For cylindrical shapes, the Reynolds number is calculated using Equation 14. [53]

$$\text{Re}_D = \frac{\rho V D}{\mu} = \frac{V D}{\nu} \quad (14)$$

The Reynolds number is closely related to the Nusselt number; however, for cylindrical vortex generators in cross flow, the relationship is not straightforward. To address this, Churchill and Bernstein (1977) proposed an empirical correlation to estimate the average Nusselt number for cross flow over a cylinder, Nu_{cyl} , incorporating both the Reynolds and Prandtl numbers, as shown in Equation 15. [53]

$$\text{Nu}_{\text{cyl}} = 0.3 + \frac{0.62 \text{Re}^{\frac{1}{2}} \text{Pr}^{\frac{1}{3}}}{\left[1 + \left(\frac{0.4}{\text{Pr}}\right)^{\frac{2}{3}}\right]^{\frac{1}{4}}} \left[1 + \left(\frac{\text{Re}}{282,000}\right)^{\frac{5}{8}}\right]^{\frac{4}{5}} \quad (15)$$

The average Nusselt number, Nu_{cyl} , has a proportional relationship with the average convective heat transfer coefficient, h , shown in Equation 16. [53]

$$\text{Nu}_{\text{cyl}} = \frac{hD}{k} \quad (16)$$

Thus, the resulting convective heat transfer coefficient, h , can be used to determine the rate of convective heat transfer, as shown in Equation 9, thereby quantifying the effect of cylindrical vortex generators on heat transfer. [30]

A 2024 study led by Z. Zhou from the University of New South Wales investigated the effect of vortex generators on photovoltaic module cooling. Zhou et al. attached rectangular wing vortex generators, made from either aluminium sheet or 3D-printed thermally conductive polymer, to the rear side of the photovoltaic modules. Although the vortex generators were optimised for free convection, both designs successfully reduced the photovoltaic module temperature by 1.5°C under low wind conditions and high irradiance. In scenarios with high module temperatures and windy conditions, the aluminium vortex generators achieved a greater cooling effect, reducing the module temperature by 2.5°C. [54]

Zhou et al.'s observation of variations in results due to different vortex generator materials highlights the significant influence of vortex generator parameters on photovoltaic module cooling. [54] As a result, several studies have investigated the influence of other vortex generator parameter modifications on the thermal performance of photovoltaic modules.

2.3.4.2. Effect of Vortex Generator Orientation on Heat Transfer

A 2023 study conducted by S. Schiffman from the University of New South Wales investigated the effect of vortex generator orientation on photovoltaic module temperature. Schiffman positioned 3D-printed vortex generators in two configurations: a forward-facing arrangement (Figure 22) and a backward-facing arrangement (Figure 23).

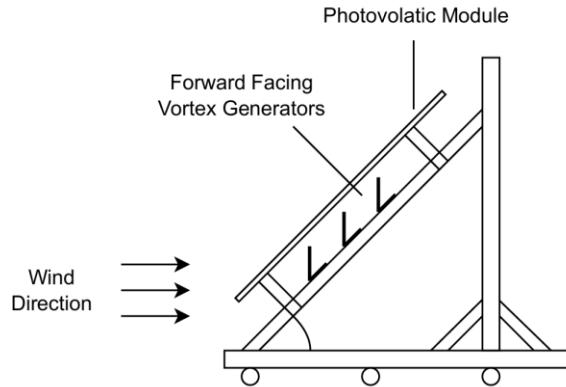


Figure 22: Forward facing vortex generator arrangement. Adapted from [55]

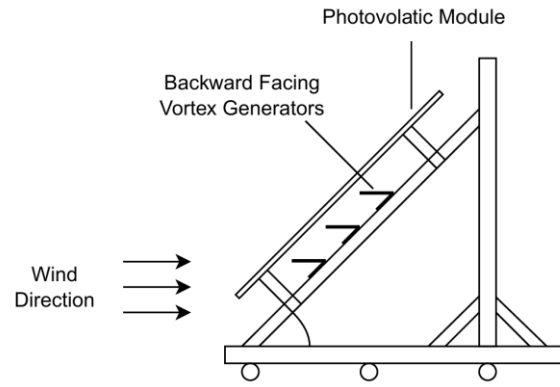


Figure 23: Backward facing vortex generator arrangement. Adapted from [55]

Schiffman's experiment revealed that although both configurations enhanced cooling of the photovoltaic module, the backward-facing arrangement consistently achieved greater temperature reductions across wind speeds of 1 m/s, 2 m/s, and 3 m/s. Specifically, the backward-facing setup achieved mean temperature reductions of approximately 1.4°C, 0.75°C, and 0.7°C, respectively. [55]

2.3.4.3. Effect of Vortex Generator Shape on Heat Transfer

Schiffman's results and experimental setup laid the foundation for further investigations into additional parameters influencing module cooling performance. Building on this work, I.R. Chaudhury examined the impact of vortex generator geometry on photovoltaic module cooling. Chaudhury tested several shapes, including cube, cylindrical, pyramid, inverted pyramid, and winglet configurations, shown in Figure 24.

While winglet-shaped vortex generators reduced photovoltaic module temperature by 5°C at 1 m/s, their free-convection based design meant that cooling effectiveness diminished at higher wind velocities. In contrast, cylindrical-shaped vortex generators demonstrated the most favourable trend, causing greater temperature reductions as the velocity increased. Thus, Chaudhury encouraged the selection of the cylindrical vortex generator for further experimentation, focusing on spacing configurations to promote turbulent flow in the span-wise direction. [56]

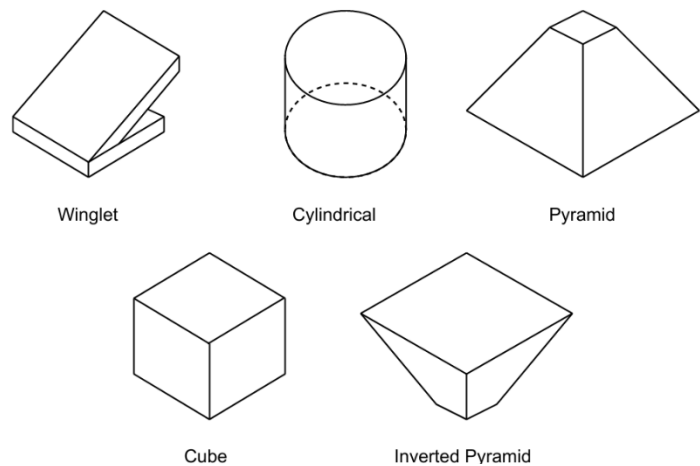


Figure 24: Vortex Generator Geometry Configurations. Adapted from [56]

2.3.4.4. Effect of Vortex Generator Spacing on Heat Transfer

Consequently, in 2024, Z. Zhao investigated the effects of span-wise, d_x , and stream-wise, d_y , spacing of cylindrical vortex generators on photovoltaic module temperature reduction. The spacing direction of the vortex generator array relative to the direction of airflow is shown in Figure 25.

For the span-wise spacing group, Zhao tested five values of horizontal spacing, d_x (26 mm, 51 mm, 102 mm, 153 mm, and 204 mm), while maintaining a constant stream-wise spacing, d_y , of 79 mm. Each configuration was subjected to forced convection wind speeds of 1.3 m/s, 2.3 m/s, and 3.3 m/s. Similarly, for the stream-wise spacing group, Zhao tested five values of vertical spacing, d_y (40 mm, 79 mm, 119 mm, 158 mm, and 198 mm), with the span-wise spacing, d_x , fixed at 51 mm. These configurations were subjected to forced convection wind speeds of 1 m/s, 2 m/s, and 3 m/s.

The results indicated that a span-wise spacing of 51 mm under a wind speed of 3.3 m/s produced the greatest temperature reduction among the span-wise configurations, achieving a decrease of 2.15°C. In the stream-wise group, a spacing of 79 mm under a wind speed of 3 m/s yielded the largest reduction, with a decrease of 2.51°C. [57]

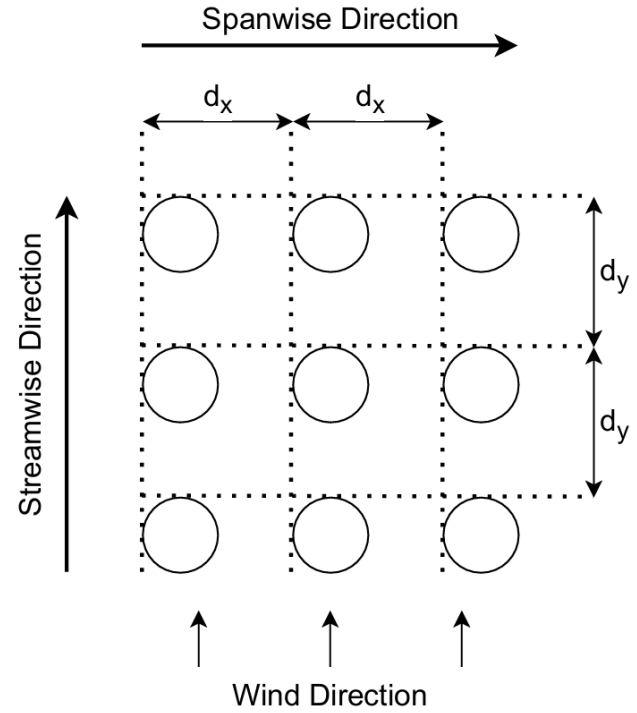


Figure 25: Spacing direction of vortex generator array relative to air direction of airflow. Adapted from [57]

2.4. Experimental Techniques

To observe the effects of vortex generators on the temperature reduction of photovoltaic modules, several experimental techniques should be considered during the experimental design process.

2.4.1. Infrared Technology

Infrared thermography is a non-invasive technique that measures mid- to long-wave infrared radiation emitted by objects and translates it into spatially resolved temperature data. [58] This technique is crucial to this thesis as it allows for the monitoring of temperature reductions in photovoltaic modules resulting from the application of cooling methods.

All bodies emit infrared radiation because of their temperature. The nature of this emission is governed by Planck's law, which states that as the temperature of a body, T_b , increases, the intensity of radiation emitted, $E_{b\lambda}$, at all wavelengths also increases. This relation is expressed in Equation 17. [59]

$$E_{b\lambda}(\lambda, T_b) = \frac{C_1}{\lambda^5 \left[\exp\left(\frac{C_2}{\lambda T_b}\right) - 1 \right]} \quad (17)$$

Thermal imaging cameras capture the emitted radiation using an infrared detector. The infrared detector then converts the radiation into an electrical signal. The most common type of infrared detector is the microbolometer, consisting of a grid of tiny sensors that measure the infrared radiation from each pixel in the scene. Each sensor element changes its electrical resistance based on the amount of radiation it absorbs. The raw data is processed and transformed into a thermal image, which is displayed on a screen.

A key advantage of infrared thermography is its non-contact nature which prevents any disturbance to the heat transfer process, ensuring that measurements remain accurate and reliable. This is particularly important in dynamic or sensitive environments where contact-based methods could alter the conditions being observed.

Therefore, infrared thermography is a useful experimental technique that will play a key role in this thesis' investigation of cooling methods for photovoltaic modules. [60]

2.4.2. Thermocouple Sensors

A thermocouple can be defined as a sensor used to measure temperature. In a thermocouple, two wires made from different metals are joined together at both ends. One of the ends is then heated, creating a continuous current that flows in the thermoelectric circuit. If the circuit is broken at the centre, the voltage across the open ends, known as the Seebeck voltage, can be measured. Since the voltage changes with temperature, the Seebeck voltage can be used to determine the temperature. [61]

Several types of thermocouples are available, each categorised by their specific temperature range. Among these, the K-type thermocouple is the most widely used, with a temperature range of -200°C to 1260°C . [62]

The broad temperature range of the K-type thermocouple enhances its versatility across a wide variety of applications. Furthermore, its relatively low-cost materials-nickel-chromium and nickel-aluminium-make it a more economical choice compared to other thermocouple types. Although the standard tolerance for a K-type thermocouple is $\pm 2.2^\circ\text{C}$ within the temperature range of 0°C to 200°C , it remains well-suited for general-purpose temperature measurements. [63]

Thus, the K-type thermocouple serves as an important experimental technique for measuring temperature reductions in photovoltaic modules.

2.4.3. Particle Image Velocimetry

Particle Image Velocimetry (PIV) is an optical measurement technique where the velocity field of an entire region within the flow is measured simultaneously. [64] Figure 26 details a typical experimental set-up of a PIV system.

The process begins with the introduction of tracer particles into the flow, a procedure commonly referred to as seeding. These particles are then illuminated within a plane or volume of the flow at least twice, separated by a short and known time interval. During these illuminations, a high-speed camera captures the light scattered by the tracer particles. The captured images are divided into small regions, known as interrogation windows. Within each window, the displacement of the particle pattern between the first and second images is analysed using a cross-correlation algorithm. By calculating the particle displacement, the velocity vector at each point can be determined, resulting in a comprehensive velocity field. [65]

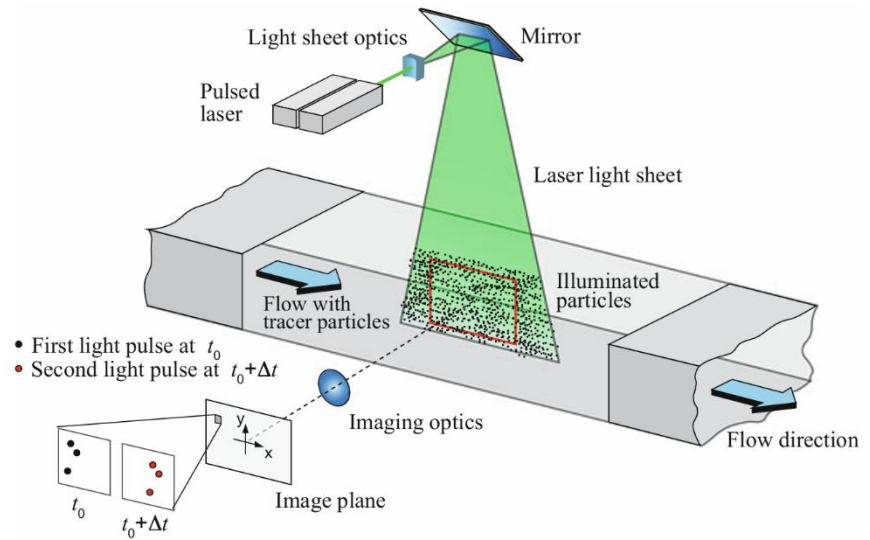


Figure 26: Experimental arrangement for planar 2C-2D PIV in a wind tunnel. Adapted from [65]

The use of PIV in investigating forced convection cooling methods for photovoltaic modules would be highly beneficial. PIV enables the visualisation of flow patterns, making it possible to identify stagnant regions where airflow is inadequate. This information can help optimise the experimental rig for better airflow performance. Furthermore, PIV reveals how objects within the wind tunnel, such as thermocouple probes and wind speed sensors, affect the flow patterns, offering insight into their effect on the photovoltaic system.

2.5. Literature Gap

The literature review in this paper initially outlined the principles governing photovoltaic modules and subsequently addressed their performance limitations. In particular, the review explored the reduction in energy conversion efficiency of photovoltaic modules at elevated temperatures.

Several conductive, radiative, and convective heat transfer methods aimed at reducing the temperature of photovoltaic modules were discussed. Of these different modes of heat transfer, convection had the greatest impact on module temperature, as most of the heat dissipation occurred through convective mechanisms. Thus, an in-depth investigation into natural and forced convective cooling methods for photovoltaic modules was undertaken, with the literature review concluding that forced convection is more effective at reducing module temperature than natural convection.

In accordance with this conclusion, several air-, water- and nanofluid-based forced convection cooling methods were examined. While it was determined that water- and nanofluid-based cooling methods outperformed air-based cooling methods, the limitations of liquid-based cooling methods in the context

of photovoltaic modules could not be overlooked. The higher initial and operational costs, increased system complexity, increased maintenance requirements and higher structural load associated with liquid-based cooling methods made air-based cooling the more realistic option for photovoltaic systems. Of the air-based cooling methods examined, vortex generators were particularly notable due to their passive cooling capability, eliminating the need for external power input as would be required with active methods such as air fans. Thus, an exploration into the effectiveness of vortex generators in cooling photovoltaic modules was conducted.

Prior to this thesis, students at the University of New South Wales investigated the effects of vortex generators on photovoltaic module temperature reduction, with each study focusing on a different parameter related to the vortex generator. To elaborate, optimal orientation, shape and spacing of vortex generators were examined under forced convection conditions. Through extensive review of these papers, in addition to other investigations into vortex generator-based cooling methods, it was determined that a lack of understanding surrounding the optimal height of vortex generators was evident. Therefore, this thesis will focus on investigating the relationship between vortex generator height and the reduction of photovoltaic module temperature under forced convection conditions.

The aims of this thesis are expressed as follows:

- I. Identify the optimal vortex generator height required to facilitate forced convective heat transfer of a photovoltaic module.
- II. Confirm existing results surrounding the ability of cylindrical vortex generators to reduce the temperature of photovoltaic modules.
- III. Further improve the vortex generator installation process by shortening set-up time.

3. Research Question and Project Plan

The research question and relevant objectives were outlined in the **Section 2.5**. The subsequent sections will detail the experimental methodology, provide a timeline for the completion of the thesis, identify the available resources, and address any required training or upskilling.

3.1. Experimental Methodology

To achieve the objectives outlined in **Section 2.5**, the experimental methodology detailed below will be applied to different height configurations of the cylindrical vortex generators (20 mm, 75 mm, and 150 mm). The Gantt charts presented in Appendix A provide a comprehensive outline of the testing plan. Experimental testing will take place in the Large Wind Tunnel (LWT) located in the Aerodynamics Laboratory at UNSW's Sydney campus was used. Owing to experimental testing conducted by previous thesis students on the effects of vortex generators on photovoltaic module temperature, the experimental rig was largely assembled, and a pre-existing testing procedure had already been established.

3.1.1. Experimental Overview

The experimental setup, shown in Figure 27, consists of a photovoltaic module mounted on a moveable platform positioned at a 45° angle relative to the horizontal. This moveable platform is placed atop a wooden base to facilitate air flow within the wind tunnel. Beneath the photovoltaic module, an acrylic roof is installed at the same angle as the module.

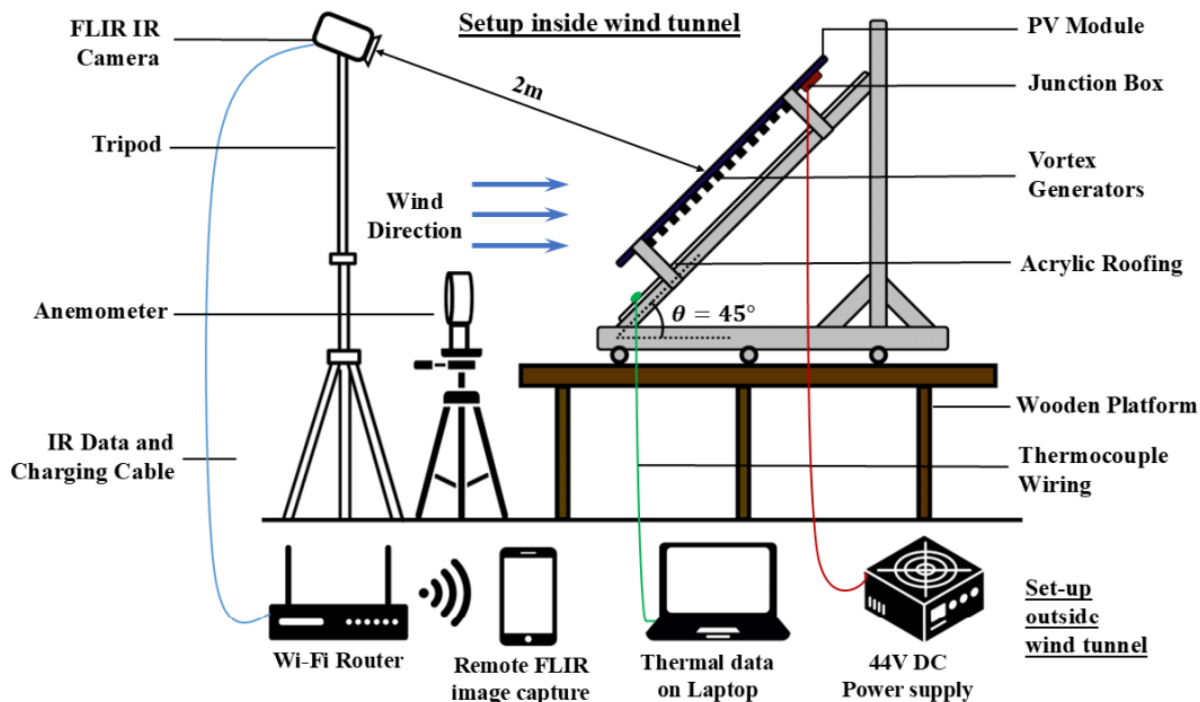


Figure 27: 2D schematic illustration of the experimental setup inside and outside the LWT section. [57]

Depending on the testing requirements, vortex generators can be installed either on the roof or directly on the photovoltaic panel; in Figure 27, the vortex generators are positioned on the panel. To power the module, the junction box is connected to a 44 V DC power supply. Module temperature is measured using thermocouple sensors, which transmit thermal data via wired connection to a laptop.

A FLIR infrared (IR) camera is positioned approximately 2 metres away from the photovoltaic module at a near-perpendicular angle. As discussed in **Section 2.4.1**, the IR camera non-invasively measures the module temperature and converts the data into thermal images. Due to the extended duration of the tests and the camera's battery limitations, the camera must remain connected to a charging cable during operation. Remote image capture is facilitated through a mobile application linked to the same Wi-Fi network as the camera.

Finally, to ensure wind speed measurements are accurate, at least one anemometer is operational throughout the experimental testing period. Placement of the anemometer at the location of the photovoltaic module within the wind tunnel allows for direct and precise wind speed monitoring.

3.1.2. Experimental Procedure

The experimental procedure is divided into four sections for clarity: experimental setup, experimental testing, post processing in FLIR and post processing in MATLAB.

3.1.2.1. Experimental Setup

The vortex generators should first be attached to either the photovoltaic panel or the acrylic roof. If they are to be installed on the panel, this must be done inside the wind tunnel, as the panel cannot be easily removed. Conversely, if the vortex generators are to be placed on the acrylic roof, installation can be completed outside the wind tunnel, since the roof is easily assembled and disassembled.

Once the vortex generators are installed, the photovoltaic module should be activated by switching on the 44 V DC power supply located outside the wind tunnel. The thermal imaging camera should then be powered on, connected to the charging cable, and positioned to capture the entire photovoltaic module. Accurate positioning can be verified using the live-stream feature available through the FLIR mobile application. It is also necessary to ensure that the anemometer is powered on and has sufficient battery life to operate for the duration of the approximately four-hour testing period.

The laptop should then be set up to receive and record the thermal data transmitted by the thermocouple sensors. After these preparations have been completed, the wind tunnel can be activated and the airflow initiated at 1 m/s.

3.1.2.2. Experimental Testing

The anemometer wind speed reading should be cross-referenced with that of the wind tunnel to ensure the airflow is maintained at 1 m/s, within an acceptable tolerance of ± 0.05 m/s. Wind speed should be checked and adjusted every 30 minutes to ensure it remains within this specified range.

Thermal image capture begins once the wind tunnel reaches steady-state conditions. For a wind speed of 1 m/s, the first thermal image should be captured using the remote FLIR image capture method 1 hour

and 50 minutes from the start of the test. The second and third images should be captured at 1 hour and 55 minutes and 2 hours, respectively, with 5-minute intervals between captures.

Following this, the wind speed should be increased to 2 m/s. After a 50-minute period to allow for thermal and flow stabilisation, the first thermal image at this speed should be captured at 2 hours and 50 minutes from the start of the test. Subsequent images should follow at 2 hours and 55 minutes and 3 hours, respectively.

The wind speed should then be increased to 3 m/s. Again, a 50-minute stabilisation period should precede image capture. The first image at this speed should be taken at 3 hours and 50 minutes, with the second and third images following at 3 hours and 55 minutes and 4 hours, respectively.

Following the capture of the third and final thermal image, the wind speed should be gradually reduced to 0 m/s before the wind tunnel is powered down. The 44 V DC power supply can then be switched off, thereby shutting down the photovoltaic module. Data collection on the laptop should be stopped, and the thermal imaging camera can be disconnected, powered down, and returned to its case. Finally, the anemometer should also be switched off.

3.1.2.3. Post Processing in FLIR

The thermal image should first be imported into FLIR's desktop application. By default, the thermal imaging camera assigns a fixed emissivity value of 0.89 and an ambient temperature of 25 °C. However, fluctuations in environmental conditions during wind tunnel operation mean that the actual ambient temperature will vary. Therefore, the ambient temperature setting should be adjusted to match the value recorded by the thermocouple at the time the thermal image was captured. Thermal temperature data is logged at a rate of 10 data sets per minute using CoolTerm. The average ambient temperature over these 10 data sets can be manually calculated and used to update the ambient temperature value within FLIR's desktop application. Once the temperature data and updated parameters have been verified, the data should be saved as a CSV file for further processing in MATLAB. This process should be repeated for all nine thermal images captured.

3.1.2.4. Post Processing in MATLAB

In MATLAB, each thermal image, which has been converted into a CSV file, is processed through a de-warping procedure. After de-warping, the processed case is compared to the corresponding de-warped baseline case. The baseline refers to experimental tests conducted under identical conditions but without the presence of vortex generators. The reduction in photovoltaic module temperature resulting from the presence of vortex generators, denoted as ΔT , is calculated by subtracting the average temperature of each photovoltaic cell within the area of interest for the baseline case, $T_{mod,baseline}$, from the average temperature of each photovoltaic cell within the corresponding area of the vortex generator case, $T_{mod,VG}$. The values of ΔT for a specific vortex generator height configuration are compiled with the results obtained for other height configurations. This data is then presented graphically to identify any trends or relationships between vortex generator height and the reduction in photovoltaic module temperature.

3.2. Thesis Timeline

All Gantt charts relating to the thesis timeline can be found in Appendix A.

Prior to Term 1, I initiated contact with my thesis supervisor, Dr Charitha de Silva, and met with PhD candidate Matthew Deng to engage in a broad discussion about the thesis. During this meeting, I was granted access to several thesis reports submitted by former students who had investigated the use of vortex generators to reduce photovoltaic module temperature. These reports were especially valuable in shaping the direction of my work, as they provided a clear sense of expectations and enabled me to identify a relevant gap in the existing literature more effectively. In addition, several supplementary research papers were recommended, allowing for considerable progress to be made on the literature review prior to the official commencement of Term 1.

3.2.1. Term 1, 2025

Given the pre-existing experimental setup established by previous thesis students, training and induction sessions were scheduled within the first few weeks of Term 1 to ensure sufficient time for preliminary setup, testing, and post-processing. Laboratory induction was booked during O-Week and was completed in the following week under the supervision of Mark Zhai. Additionally, training in equipment operation and post-processing was conducted by Matthew Deng across Weeks 1 to 3. Consequently, by Week 4 of Term 1, all preparatory requirements for commencing preliminary setup, testing, and post-processing had been fulfilled.

In Week 2, the identification of a literature gap allowed part orders to begin. Vortex generators, measuring 20 mm in diameter and 75 mm in height, were designed and ordered from the ENG Makerspace. They were needed as soon as possible, as they were essential for setting up the experimental rig. Later in the term, vortex generators with the same diameter but a height of 150 mm were ordered using the same process. However, due to technical issues with the 3D printers at the ENG Makerspace, these parts were scheduled for completion in Week 10 of Term 1. This delay did not impact on the progress of testing, as no specific expectations had been set regarding the number of tests to be conducted during Term 1.

Figure 32 observes the scheduling of preliminary setup, testing and post-processing immediately following the completion of the required laboratory induction and relevant training sessions. This approach was adopted to maximise the available time for gaining experience in conducting tests. However, due to the presence of multiple noise-sensitive experiments in the same laboratory as the wind tunnel, test sessions were occasionally postponed to avoid interference—an occurrence that was not uncommon. Furthermore, various issues may arise during the experimental process, potentially compromising the integrity of the data and necessitating retests, which could significantly delay the progression of the thesis. To accommodate such delays, buffer periods were incorporated into the subsequent Gantt charts. Given the limited initial experience with test procedures, no specific expectations were set for the number of tests to be conducted in Term 1. As a result, a buffer period was not included in the Gantt chart for that term.

As previously mentioned, the literature review process commenced during O-Week of Term 1. Given the iterative nature of conducting a comprehensive literature review, continuous revisions were necessary as new information emerged. Accordingly, time was allocated throughout the duration of Term 1 for this task, except for the final week, which was reserved for finalisation and submission.

Moreover, the development of the Thesis A report progressed in parallel with the formation of the literature review. As such, the drafting of the report was scheduled from Week 1 through to Week 9 of Term 1. The initial submission date was set for Friday the 25th of April; however, due to public holidays during that period, the deadline was later extended to Monday the 28th of April.

3.2.2. Term 1-2 Break, 2025

During the month-long break between the first and second trimesters, a window of opportunity became available from the 28th of April to the 16th of May for experimental testing in the Aerodynamics laboratory, free from interruptions caused by noise-sensitive experiments. Therefore, Shubhneet Sodhi and I plan to take advantage of this period to conduct most of the roof-based tests.

Shubhneet's research involves testing both staggered and aligned configurations, whereas my work focuses solely on the aligned configuration. To streamline the testing process and minimise setup time between trials, the experimental arrangement alternates between aligned and staggered configurations, as shown in Figure 33.

Based on experience gained during Term 1, setting up a test takes approximately one hour, with each test running for about four hours and post-processing requiring an additional hour. This means that testing and post-processing for one configuration, along with setting up for the next, can be completed within a single day. As a result, 4–5 tests have been scheduled per week during the available timeframe.

It is not feasible to complete all roof-based tests during this available timeframe. As such, the remaining tests are scheduled for the early weeks of Term 2. Buffer periods are incorporated at the end of specific test categories, namely, roof-based and panel-based tests, to accommodate unforeseen delays. Accordingly, a buffer period for roof-based testing has been allocated in the Term 2 Gantt chart, rather than in the Term 1–2 Break Gantt chart.

3.2.3. Term 2, 2025

The Term 2 Gantt chart, shown in Figure 34, outlines the completion of the remaining roof-based tests. As previously discussed, a three-week buffer period has been allocated following their expected completion to accommodate any unforeseen delays. Consequently, under a worst-case scenario, panel-based testing is scheduled to commence in Week 5 of Term 2.

Given the current uncertainty around laboratory scheduling, a conservative maximum estimate of five tests every two weeks has been planned for Terms 2 and 3. This approach is intended to set realistic expectations regarding the number of tests that can feasibly be completed.

Similar to the structure of the Thesis A report, the Thesis B report has been divided into a drafting phase and a submission phase. For students completing their Thesis B during Term 1 of 2025, the submission

deadline is Week 10. Accordingly, an estimated submission date of Week 10 in Term 2 has been incorporated into the Term 2 Gantt chart for my Thesis B report.

3.2.4. Term 3, 2025

Finally, the Term 3 Gantt chart, presented in Figure 35, estimates the completion of the panel-based tests by the end of Week 1 of Term 3. As with the roof-based tests, a three-week buffer period has been allocated following the completion of the panel-based tests.

The time allocated for drafting the Thesis C report mirrors that of the Thesis B report, spanning from O-Week to Week 9, with an expected submission date in Week 10. The preparation for the Thesis C presentation is scheduled to begin in Week 5 of Term 3, as all tests are anticipated to be completed by then, assuming the worst-case scenario in which both buffer periods are required in full. The expected submission date for the Thesis C presentation is set for Week 10 of Term 3, based on the timelines established in previous terms.

3.3. Available Resources Identified

Several resources have been made available to support the completion of my thesis.

3.3.1. Technical Resources

As mentioned in **Section 3.2**, Thesis C reports by Sophie Schiffman, Ishan Chaudhury, and Ziao Zhou, provided by Dr. Charitha de Silva, were helpful for my literature review and overall thesis development. UNSW-based research papers on vortex generators also served as a valuable starting point, along with online research papers accessible for free or via university email accounts. The UNSW Library provided helpful textbooks, especially for the heat transfer section of the literature review, aiding in the revision of fundamental concepts. University-provided software, including Adobe Creative Cloud, Microsoft Office, GitHub, and OneDrive, streamlined the report-writing process. Furthermore, SolidWorks and the ENG Makerspace were responsible for the design and 3D printing of the vortex generators. For experimental testing, FLIR thermal imaging is used. The system includes a thermal camera aimed at the photovoltaic module, a mobile app for remote image capture, and a desktop app for initial post-processing. MATLAB is used to analyse FLIR-generated CSV files and determine temperature changes in the photovoltaic modules. Finally, testing is conducted in the 201/202 Aerodynamics Lab, located in the Ainsworth Building (J17) on UNSW's Sydney Campus.

3.3.2. Human Resources

Mark Zhai is the Lab Technical Officer in the Aerodynamics Lab and serves as my first point of contact should any issues arise during my time there. Matthew Deng, a PhD student whose research on the effects of vortex generators on photovoltaic module temperature overlaps with my own, has extensive experience in the testing process. His expertise provides valuable insight into experimental setup, testing, and post-processing. Dr. Charitha de Silva is my thesis advisor. During our weekly meetings, we discuss the relevant literature, testing strategies, and various other topics related to the progression of my thesis. These weekly meetings provide a key opportunity to review progress and ensure the thesis is advancing in the right direction. Finally, Dr. Tracie Barber is the course convenor for the mechanical and

manufacturing engineering thesis stream. Any course-related concerns can be addressed through the designated Microsoft Teams channel or via email.

3.4. Required training and upskilling identified

Required training to access the Aerodynamics Lab needed to be identified and completed prior to preliminary testing. In addition, training and upskilling of experiment-specific processes also needed to be undertaken.

3.4.1. Aerodynamics Lab

Access to the J18 201/202 Aerodynamics Laboratory was contingent upon the successful completion of a Health, Safety, and Environment (HSE) orientation quiz, which required a perfect score of 100%. Upon passing the quiz, the requisite online training modules specific to the Aerodynamics Laboratory were required, shown in Table 2.

Table 2: Required courses for laboratory access. [66]

Required Enrolment	Course Name	Course Code	Delivery Method
All Lab Users	Safety@UNSW	SAFETYUNSW	Online
	Lab Health and Safety	SAFETYLABS	Online
	Hazardous Chemicals	SAFETYCHEM	Online
Lab working requires use of fume cupboard	Fume Cupboards & Safety	SAFETYFUME	Online
If working in Class 3B or Class 4 Laser labs	UNSW Laser Safety Awareness	N/a	Online
	Laser Safety for Operator Course (for Research students)	N/a	Online
	1 Day Laser Safety Level 2 (for staff)	N/a	By edVirtus
	5 Day Laser Safety Level 1 (for laser safety officer)	N/a	By edVirtus

In accordance with the requirements of the Aerodynamics Laboratory and the nature of the equipment used for experimental testing, it was recommended that the following courses be completed: *Safety@UNSW*, *Lab Health and Safety*, and *Hazardous Chemicals*.

Following the completion of these modules, an in-person induction into the Aerodynamics Lab is required under the supervision of the Lab Technical Officer, Mark Zhai.

3.4.2. Experimental Setup, Testing and Post Processing

To ensure the successful execution of experimental tests, training was required in setting up the testing environment, conducting the tests, and performing post-processing. This training was provided by Matthew Deng through a comprehensive demonstration of the entire testing procedure. Specifically, the training involved detailed guidance on assembling the vortex generators onto the experimental rig, setting up and operating the thermal imaging camera and wind-speed readers, using the laptop for data acquisition during testing, operating the wind tunnel, as well as performing post-processing using both FLIR software and MATLAB-based tools.

4. Project Dependent Preparations

4.1. Evidence of training on specific equipment

As outlined in **Section 3.4.1**, the HSE quiz, required online courses, and in-person laboratory induction were all mandatory prerequisites for commencing experimental testing. Documentation confirming their completion can be found in Appendix B.

4.2. Evidence of some upskill in new software/methods

Due to the experiment-specific use of the FLIR software, no additional training was recommended beyond the initial demonstration. Furthermore, given a background in Computer Science and prior experience with MATLAB through coursework, only minimal revision of MATLAB concepts was conducted. [67]

4.3. Preliminary results (Aligned 75 mm VG Positioned on Roof)

Figures 28, 29, and 30 illustrate the isometric, front, and side views of the preliminary experimental test, in which 75 mm vortex generators were placed on the roof.



Figure 28: Isometric View of Experimental Rig

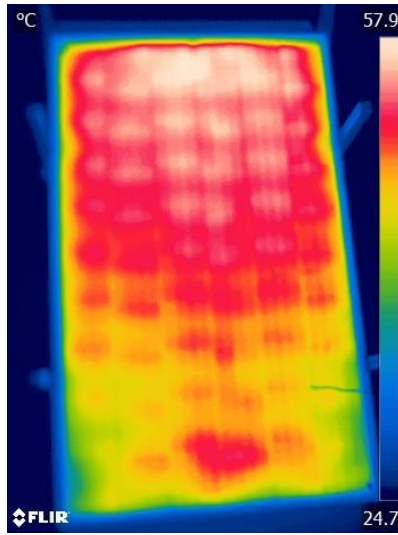


Figure 29: Front View of Experimental Rig



Figure 30: Side View of Experimental Rig

Figure 31 exemplifies the result of post processing using FLIR for one of the nine thermal image captures. The reflective temperature was changed using the thermocouple measurements shown in Table 3.



File Name: Cylinder_75_Roof_1ms1	
Parameters:	
Emissivity	0.89
Refl. Temp (T_{amb})	25°C → 25.4°C
Distance	2 m
Atmospheric Temp	25.4°C
Ext. optics temp	20°C
Ext. optics trans	1
Relative humidity	40%
IR resolution	348 x 464
Date created	202/10/4 9:31:15

Figure 31: Thermal Image Capture and Corresponding Parameters (Cylinder_75_Roof_1ms1)

Table 3: Thermocouple data recorded used to find the average reflection temperature.

Date	Timestamp	Humidity %	Refl. Temp (T_{amb}) °C
07/04/2025	13:40:02	39.50	25.43
07/04/2025	13:40:07	39.50	25.40
07/04/2025	13:40:13	39.50	25.40
07/04/2025	13:40:19	39.60	25.40
07/04/2025	13:40:25	39.60	25.40
07/04/2025	13:40:30	39.60	25.43
07/04/2025	13:40:36	39.60	25.40
07/04/2025	13:40:42	39.60	25.40
07/04/2025	13:40:48	39.70	25.36
07/04/2025	13:40:54	39.70	25.40

Table 4 presents the change in temperature of the photovoltaic module during experimental testing across various wind speeds, with negative values indicating module cooling. Contrary to expectations, the vortex generators generally resulted in an increase in module temperature during operation, except for the ninth image capture. A discussion with Matthew Deng suggested that an error likely occurred either during the experimental procedure or during post-processing. The next step will be to determine the cause of this discrepancy.

Table 4: Resultant Data for Cylinder_75_Roof_1ms1 case.

Wind Speed (m/s)	Time of Image Capture (min)	Change in Temperature, ΔT , ($^{\circ}\text{C}$)
1	110	9.1687
1	115	9.1344
1	120	8.9427
2	170	3.7623
2	175	3.5636
2	180	2.0595
3	230	0.1515
3	235	0.0468
3	240	-0.1204

4.4. Components/parts ordered

As mentioned previously in **Section 3.2**, the experimental rig had already been assembled by previous thesis students. Consequently, only a minimal number of components were ordered during Term 1, and no additional parts are currently expected to be ordered. Table 5 outlines the relevant components and parts, the quantities required, and their status.

Table 5: Components/parts ordered.

Component	Quantity	Status
Pitot Tube Anemometer	1	Ordered and installed on the experimental testing rig.
Cylindrical Vortex Generators (20 mm Diameter, 20 mm Height)	200	Already 3D printed as part of a previous student's thesis. [56]
Cylindrical Vortex Generators (20 mm Diameter, 75 mm Height)	200	Ordered, 3D printed and collected.
Cylindrical Vortex Generators (20 mm Diameter, 150 mm Height)	200	Ordered, 3D printed and collected.

4.5. Detailed budget of parts to be ordered

The cost of the parts to be ordered detailed in Table 5 are outlined in Table 6. The cost of the 3D-printed cylindrical vortex generators was estimated based on their volume and the price of PLA filament. [68] Additionally, the Pitot Tube Anemometer was approximated at 400 AUD, based on comparable products available online. [69]

Table 6: Detailed budget of parts to be ordered.

Component	Weight per Part (kg)	Quantity	Total Weight (kg)	Cost (\$)
Pitot Tube Anemometer	N/a	1	N/a	400
Cylindrical Vortex Generators (20 mm Diameter, 20 mm Height)	0.0314	200	6.2831	1154.54
Cylindrical Vortex Generators (20 mm Diameter, 75 mm Height)	0.1178	200	23.5619	
Cylindrical Vortex Generators (20 mm Diameter, 150 mm Height)	0.2356	200	47.1239	
			Total Cost (\$)	1554.54

4.6. Risk Assessment

A comprehensive risk assessment was undertaken due to the experimental testing scheduled in the Aerodynamics Laboratory. This assessment accounted for both experiment-specific hazards and general risks associated with the laboratory environment, as detailed in Appendix C. All identified risks were classified as either medium or low, indicating a relatively safe working environment, provided that all existing control measures are properly implemented.

5. Conclusion

The transition to sustainable energy sources in recent years has propelled photovoltaic modules to the forefront of renewable energy research. Consequently, extensive efforts have been dedicated to mitigating the decline in module efficiency at elevated temperatures. Following an exploration of the fundamental principles governing photovoltaic module operation and their associated performance limitations, this thesis critically examined a range of methods aimed at reducing module temperatures during operation.

The effectiveness of conduction-, radiation-, and convection-based cooling strategies was evaluated, with convection emerging as the most promising approach. In particular, forced convection techniques demonstrated the greatest effectiveness in lowering photovoltaic module temperatures. This finding prompted a focused investigation into air-, water-, and nanofluid-based cooling methods under forced convection conditions, wherein air-based strategies were identified as the most suitable for practical implementation.

Among air-based cooling approaches, the use of vortex generators emerged as a highly effective passive cooling method. Accordingly, this research examined the influence of vortex generator parameters on photovoltaic module cooling performance. Specifically, prior studies addressing vortex generator orientation, shape, and spacing were reviewed. However, a notable gap in the literature regarding the effect of vortex generator height on temperature reduction was identified.

As a result, an experimental plan was developed to evaluate the impact of varying vortex generator heights on the cooling performance of photovoltaic modules. The next phase of this research will involve the execution of this plan, employing vortex generators with heights of 20 mm, 75 mm, and 150 mm.

References

- [1] ClientEarth, “Fossil fuels and climate change: the facts,” ClientEarth. Accessed: Apr. 26, 2025. [Online]. Available: https://www.clientearth.org/latest/news/fossil-fuels-and-climate-change-the-facts/?utm_source=chatgpt.com
- [2] World Health Organization, “Ambient (outdoor) air pollution,” World Health Organization. Accessed: Apr. 26, 2025. [Online]. Available: https://www.who.int/news-room/fact-sheets/detail/ambient-%28outdoor%29-air-quality-and-health?utm_source=chatgpt.com
- [3] ExxonMobil, “Energy supply,” ExxonMobil. Accessed: Apr. 26, 2025. [Online]. Available: https://corporate.exxonmobil.com/sustainability-and-reports/global-outlook/energy-supply?utm_source=chatgpt.com
- [4] IEA, “Electricity 2024,” IEA. Accessed: Apr. 26, 2025. [Online]. Available: Electricity 2024
- [5] W. Shockley and H. J. Queisser, “Detailed Balance Limit of Efficiency of p-n Junction Solar Cells,” *J Appl Phys*, vol. 32, pp. 510–519, Mar. 1961.
- [6] S. Dubey, J. N. Sarvaiya, and B. Seshadri, “Temperature dependent photovoltaic (PV) efficiency and its effect on PV production in the world - A review,” in *Energy Procedia*, Nanyang: Elsevier Ltd, 2013, pp. 311–321. doi: 10.1016/j.egypro.2013.05.072.
- [7] H. G. Teo, P. S. Lee, and M. N. A. Hawlader, “An active cooling system for photovoltaic modules,” *Appl Energy*, vol. 90, no. 1, pp. 309–315, 2012, doi: 10.1016/j.apenergy.2011.01.017.
- [8] Morgan King, “The Impact of Heatwaves on Solar Panels,” Morgan King. Accessed: Apr. 26, 2025. [Online]. Available: <https://www.morganking.co.uk/blogposts/the-impact-of-heatwaves-on-solar-panels/>
- [9] Enel Green Power, “Photovoltaic module,” Enel Green Power. Accessed: Mar. 07, 2025. [Online]. Available: <https://www.enelgreenpower.com/learning-hub/renewable-energies/solar-energy/photovoltaic-module>
- [10] U.S. DEPARTMENT of ENERGY, “Solar Photovoltaic Technology Basics,” U.S. DEPARTMENT of ENERGY. Accessed: Mar. 07, 2025. [Online]. Available: <https://www.energy.gov/eere/solar/solar-photovoltaic-technology-basics>
- [11] Science ABC, “Photoelectric Effect Explained in Simple Words for Beginners,” Science ABC. Accessed: Mar. 08, 2025. [Online]. Available: <https://www.youtube.com/watch?v=H-FyOpURPXI>

- [12] U.S. DEPARTMENT of ENERGY, “Solar Photovoltaic Cell Basics,” U.S. DEPARTMENT of ENERGY. Accessed: Mar. 08, 2025. [Online]. Available: <https://www.energy.gov/eere/solar/solar-photovoltaic-cell-basics#:~:text=Silicon%20is%2C%20by%20far%2C%20the,semiconductor%20used%20in%20computer%20chips.>
- [13] CircuitBread, “Classification of Semiconductors (Intrinsic/Extrinsic, P-Type/N-Type),” CircuitBread. Accessed: Apr. 21, 2025. [Online]. Available: https://www.youtube.com/watch?v=ErcH_OuCaNY
- [14] P. Gupta and S. Mata Vaishno, “Solar EV Chargers and Super Flow Batteries for an Efficient Electric Vehicle,” *International Research Journal of Engineering and Technology*, 2020.
- [15] TED-Ed, “How do solar panels work? - Richard Komp,” TED-Ed. Accessed: Mar. 08, 2025. [Online]. Available: <https://www.youtube.com/watch?v=xKxrkt7CpY>
- [16] A. H. W. Il, “The Theory of Electronic Semi-Conductors,” Cambridge, Jun. 1931. [Online]. Available: <https://royalsocietypublishing.org/>
- [17] CircuitBread, “Band Gap and Semiconductor Current Carriers | Intermediate Electronics,” CircuitBread. Accessed: Mar. 15, 2025. [Online]. Available: https://www.youtube.com/watch?v=N8MuD_xu6L4
- [18] Renewable_Tek, “HOT Days, LESS POWER? Solar Panel Temperature Coefficient Explained!,” Renewable_Tek. Accessed: Mar. 15, 2025. [Online]. Available: <https://www.youtube.com/watch?v=9j9NxrZOWf4>
- [19] C. Honsberg and S. Bowden, “Solar Cell Efficiency,” PVEducation. Accessed: Mar. 15, 2025. [Online]. Available: <https://www.pveducation.org/pvcdrom/solar-cell-operation/solar-cell-efficiency>
- [20] P. Baruch, A. De Vos, P. T. Landsberg, and J. E. Parrott, “On some thermodynamic aspects of photovoltaic solar energy conversion,” *Solar Energy Materials and Solar Cells*, vol. 36, no. 2, pp. 201–222, Feb. 1995, doi: 10.1016/0927-0248(95)80004-2.
- [21] M. Y. Levy and C. Honsberg, “Rapid and precise calculations of energy and particle flux for detailed-balance photovoltaic applications,” *Solid State Electron*, vol. 50, no. 7–8, pp. 1400–1405, Jul. 2006, doi: 10.1016/J.SSE.2006.06.017.
- [22] C. Honsberg and S. Bowden, “Open-Circuit Voltage,” PVEducation. Accessed: Mar. 14, 2025. [Online]. Available: https://www.pveducation.org/pvcdrom/solar-cell-operation/open-circuit-voltage#footnote3_r1kip45

- [23] C. Honsberg and S. Bowden, “Short-Circuit Current,” PVEducation. Accessed: Mar. 16, 2025. [Online]. Available: <https://www.pveducation.org/pvcdrom/solar-cell-operation/short-circuit-current>
- [24] M. A. Green, “Solar cell fill factors: General graph and empirical expressions,” Sydney, Jan. 1981.
- [25] A. Dolara, G. C. Lazaroïu, S. Leva, and G. Manzolini, “Experimental investigation of partial shading scenarios on PV (photovoltaic) modules,” *Energy*, vol. 55, pp. 466–475, Jun. 2013, doi: 10.1016/J.ENERGY.2013.04.009.
- [26] E. Asl-Soleimani, S. Farhangi, and M. S. Zabihi, “The effect of tilt angle, air pollution on performance of photovoltaic systems in Tehran,” *Renew Energy*, vol. 24, no. 3–4, pp. 459–468, Nov. 2001, doi: 10.1016/S0960-1481(01)00029-5.
- [27] K. Hasan, S. B. Yousuf, M. S. H. K. Tushar, B. K. Das, P. Das, and M. S. Islam, “Effects of different environmental and operational factors on the PV performance: A comprehensive review,” Feb. 01, 2022, *John Wiley and Sons Ltd, London*. doi: 10.1002/ese3.1043.
- [28] C. Honsberg and S. Bowden, “Heat Loss in PV Modules,” PVEducation. Accessed: Mar. 31, 2025. [Online]. Available: <https://www.pveducation.org/pvcdrom/modules-and-arrays/heat-loss-in-pv-modules>
- [29] P. Dwivedi, K. Sudhakar, A. Soni, E. Solomin, and I. Kirpichnikova, “Advanced cooling techniques of P.V. modules: A state of art,” *Case Studies in Thermal Engineering*, vol. 21, p. 100674, Oct. 2020, doi: 10.1016/J.CSITE.2020.100674.
- [30] Y. A. Çengel and A. J. Ghajar, “Introduction and Basic Concepts,” in *Heat and Mass Transfer: Fundamentals and Applications*, 5th ed., New York: McGraw-Hill, 2014, ch. 1, pp. 2–38.
- [31] V. Kumar and C. Shakher, “Qualitative and quantitative investigations of temperature distribution, heat flow, and heat transfer parameters from the heated objects using lensless Fourier transform digital holography: A review,” *Opt Laser Technol*, vol. 168, Jan. 2024, doi: 10.1016/j.optlastec.2023.109918.
- [32] S. N. Razali *et al.*, “Performance enhancement of photovoltaic modules with passive cooling multidirectional tapered fin heat sinks (MTFHS),” *Case Studies in Thermal Engineering*, vol. 50, p. 103400, Oct. 2023, doi: 10.1016/J.CSITE.2023.103400.
- [33] A. F. Nicholas, M. Z. Hussein, Z. Zainal, and T. Khadiran, “Activated Carbon for Shape-Stabilized Phase Change Material,” in *Synthesis, Technology and Applications of Carbon Nanomaterials*, 1st ed., Amsterdam: Elsevier, 2019, ch. 12, pp. 279–308. doi: 10.1016/B978-0-12-815757-2.00013-9.

- [34] B. Hussain, H. W. Malik, F. U. Hasnain, and M. Irfan, "Phase Change Material for the Cooling of Solar Panels—An Experimental Study †," *Engineering Proceedings*, vol. 45, no. 1, 2023, doi: 10.3390/engproc2023045043.
- [35] J. Song, J. Seo, J. Han, J. Lee, and B. J. Lee, "Ultrahigh emissivity of grating-patterned PDMS film from 8 to 13 μ m wavelength regime," *Appl Phys Lett*, vol. 117, no. 9, Aug. 2020.
- [36] B. Zhao, M. Hu, X. Ao, and G. Pei, "Performance analysis of enhanced radiative cooling of solar cells based on a commercial silicon photovoltaic module," *Solar Energy*, vol. 176, pp. 248–255, Dec. 2018, doi: 10.1016/J.SOLENER.2018.10.043.
- [37] Y. A. Çengel and A. J. Ghajar, "Fundamentals of Convection," in *Heat and Mass Transfer: Fundamentals and Applications*, 5th ed., New York: McGraw-Hill, 2014, ch. 6, pp. 387–390.
- [38] B. Zohuri, "Thermosyphon and heat pipe applications," *Functionality, Advancements and Industrial Applications of Heat Pipes*, pp. 307–344, 2020, doi: 10.1016/B978-0-12-819819-3.00006-7.
- [39] A. R. Abdulmunem, P. Mohd Samin, H. Abdul Rahman, H. A. Hussien, I. Izmi Mazali, and H. Ghazali, "Numerical and experimental analysis of the tilt angle's effects on the characteristics of the melting process of PCM-based as PV cell's backside heat sink," *Renew Energy*, vol. 173, pp. 520–530, Aug. 2021, doi: 10.1016/J.RENENE.2021.04.014.
- [40] Y. A. Çengel and A. J. Ghajar, "Natural Convection," in *Heat and Mass Transfer: Fundamentals and Applications*, 5th ed., New York: McGraw-Hill, 2014, ch. 9, pp. 533–579.
- [41] S. Basu, "Mass Flow Meter," in *Plant Flow Measurement and Control Handbook*, Amsterdam: Elsevier, 2019, ch. 6, pp. 541–613. doi: 10.1016/B978-0-12-812437-6.00006-8.
- [42] International Electrotechnical Commission, "IEC 61215:2005 - Crystalline silicon terrestrial photovoltaic (PV) modules - Design qualification and type approval," International Electrotechnical Commission. Accessed: Apr. 12, 2025. [Online]. Available: <https://www.iecee.org/certification/iec-standards/iec-612152005#:~:text=Lays%20down%20requirements%20for%20the,IEC%2060721%2D2%2D1.>
- [43] A. Almuwailhi and O. Zeitoun, "Investigating the cooling of solar photovoltaic modules under the conditions of Riyadh," *Journal of King Saud University - Engineering Sciences*, vol. 35, no. 2, pp. 123–136, Feb. 2023, doi: 10.1016/J.JKSUES.2021.03.007.

- [44] I. Al-Masalha, A. S. Alsabagh, O. Badran, N. Alkawaldeh, T. M. Abu-Rahmeh, and A. Al Alawin, “Improving photovoltaic module efficiency using water sprinklers, air fans, and combined cooling systems,” *EPJ Photovoltaics*, vol. 15, Oct. 2024, doi: 10.1051/epjpv/2024037.
- [45] T. K. Murtadha, A. A. Dil Hussein, A. A. H. Alalwany, S. S. Alrwashdeh, and A. M. Al-Falahat, “Improving the cooling performance of photovoltaic panels by using two passes circulation of titanium dioxide nanofluid,” *Case Studies in Thermal Engineering*, vol. 36, p. 102191, Aug. 2022, doi: 10.1016/J.CSITE.2022.102191.
- [46] A. K. Suresh, S. Khurana, G. Nandan, G. Dwivedi, and S. Kumar, “Role on nanofluids in cooling solar photovoltaic cell to enhance overall efficiency,” *Mater Today Proc*, vol. 5, no. 9, pp. 20614–20620, Jan. 2018, doi: 10.1016/J.MATPR.2018.06.442.
- [47] M. Samykano, “Hybrid Photovoltaic Thermal Systems: Present and Future Feasibilities for Industrial and Building Applications,” *Buildings*, vol. 13, no. 8, Aug. 2023, doi: 10.3390/buildings13081950.
- [48] E. Ponticorvo, M. Iuliano, C. Cirillo, A. Maiorino, C. Aprea, and M. Sarno, “Fouling Behavior and Dispersion Stability of Nanoparticle-Based Refrigeration Fluid,” *Energies (Basel)*, vol. 15, no. 9, May 2022, doi: 10.3390/en15093059.
- [49] A. Sakanova, C. F. Tong, A. Nawawi, R. Simanjorang, K. J. Tseng, and A. K. Gupta, “Investigation on weight consideration of liquid coolant system for power electronics converter in future aircraft,” *Appl Therm Eng*, vol. 104, pp. 603–615, Jul. 2016, doi: 10.1016/j.applthermaleng.2016.05.097.
- [50] M. Awais and A. A. Bhuiyan, “Heat transfer enhancement using different types of vortex generators (VGs): A review on experimental and numerical activities,” *Thermal Science and Engineering Progress*, vol. 5, pp. 524–545, Mar. 2018, doi: 10.1016/J.TSEP.2018.02.007.
- [51] K. Van Treuren, “ABSTRACT Design and Experimental Testing of Small-Scale Wind Turbines,” Waco, Aug. 2015. [Online]. Available: <https://www.researchgate.net/publication/265745889>
- [52] R. Wille, “Kármán Vortex Streets,” *Advances in Applied Mechanics*, vol. 6, no. C, pp. 273–287, Jan. 1960, doi: 10.1016/S0065-2156(08)70113-3.
- [53] Y. A. Çengel and A. J. Ghajar, “External Forced Convection,” in *Heat and Mass Transfer: Fundamentals and Applications*, 5th ed., New York: McGraw-Hill, 2014, ch. 7.
- [54] Z. Zhou, A. Gentle, M. Mohsenzadeh, Y. Jiang, M. Keevers, and M. Green, “Long-term outdoor testing of vortex generators for passive PV module cooling,” *Solar Energy*, vol. 275, p. 112610, Jun. 2024, doi: 10.1016/J.SOLENER.2024.112610.

- [55] S. Schiffmann, “An Investigation into the Effectiveness of Vortex Generator Cooling on Photovoltaic Modules under Forced Convection Conditions,” Sydney, Nov. 2023.
- [56] I. R. Chaudhury, “The cooling effects of vortex generators to increase efficiency on Photovoltaic modules under forced convection,” Sydney, Apr. 2024.
- [57] Z. Zhou, “Spacing Effect of Vortex Generator Array on PV Module Cooling in Forced Convection,” Sydney, Nov. 2024.
- [58] G. J. Tattersall, “Infrared thermography: A non-invasive window into thermal physiology,” *Comp Biochem Physiol A Mol Integr Physiol*, vol. 202, pp. 78–98, Dec. 2016, doi: 10.1016/J.CBPA.2016.02.022.
- [59] Y. A. Çengel and A. J. Ghajar, “Fundamentals of Thermal Radiation,” in *Heat and Mass Transfer: Fundamentals and Applications*, 5th ed., New York: McGraw-Hill, 2014, ch. 12, pp. 717–810.
- [60] History of Simple Things, “How Does a Thermal Imaging Camera Work?,” History of Simple Things. Accessed: Apr. 20, 2025. [Online]. Available: <https://www.youtube.com/watch?v=6UAFCCzV874&t=294s>
- [61] Omega Engineering, “Thermocouples | OMEGA Engineering,” Omega Engineering. Accessed: Apr. 21, 2025. [Online]. Available: <https://au.omega.com/prodinfo/thermocouples.html#:~:text=A%20thermocouple%20is%20a%20sensor,device%20at%20the%20other%20end.>
- [62] The Engineering Mindset, “How Thermocouples Work - basic working principle + RTD,” The Engineering Mindset. Accessed: Apr. 21, 2025. [Online]. Available: <https://www.youtube.com/watch?v=v7NUi88Lxi8&t=19s>
- [63] ETW International, “KX Thermocouple Extension Wire (Silicone Rubber Insulated Wire 2X7/0.2mm),” ETW International. Accessed: Apr. 21, 2025. [Online]. Available: <https://etwinternational.com/1-1-21-silicone-rubber-thermocouple-extension-wire181801-61282.html>
- [64] M. D. Atkins, “Velocity Field Measurement Using Particle Image Velocimetry (PIV),” *Application of Thermo-Fluidic Measurement Techniques: An Introduction*, pp. 125–166, Jul. 2016, doi: 10.1016/B978-0-12-809731-1.00005-8.
- [65] M. Raffel, C. E. Willert, F. Scarano, C. J. Kähler, S. T. Wereley, and J. Kompenhans, *Particle Image Velocimetry: A Practical Guide (Third Edition)*, 3rd ed. Cham: Springer International Publishing, 2018.
- [66] University of New South Wales, “Lab access how-to,” UNSW. Accessed: Jan. 07, 2025. [Online]. Available: <https://www.unsw.edu.au/engineering/our-schools/mechanical-and-manufacturing-engineering/resources/lab-access>

- [67] N. Sivalingam, "Evidence of Prior MATLAB Experience," GitHub. Accessed: Apr. 27, 2025. [Online]. Available: <https://github.com/nathansivalingam/space-systems-architecture-matlab>
- [68] Jaycar, "Creality Ender-PLA 1.75mm Black PLA Prototyping Filament 1kg Roll," Jaycar. Accessed: Apr. 27, 2025. [Online]. Available: https://www.jaycar.com.au/creality-ender-pla-1-75mm-black-pla-prototyping-filament-1kg-roll/p/TL4801?gad_source=1&gad_campaignid=21876842869&gbraid=0AAAAAD0dvLaZAKxKPqxYhxUvYoY2TC92g&gclid=CjwKCAjwq7fABhB2EiwAwk-YbD9zcTTc6fJdg-pVlp1Ox9APNq-x-rBtQNk1AMJVtU0hAMrq7glPwhoCKusQAvD_BwE
- [69] HVAC DIRECT, "Testo 405i - Hot-wire Anemometer Wireless Smart Probe - Smartphone Operation," HVAC DIRECT. Accessed: Apr. 27, 2025. [Online]. Available: http://hvacdirect.com.au/products/testo-405i-hot-wire-anemometer-wireless-smart-probe?variant=49664802881855&country=AU¤cy=AUD&utm_medium=product_sync&utm_source=google&utm_content=sag_organic&utm_campaign=sag_organic&gad_source=1&gad_campaignid=17144211308&gbraid=0AAAAADMCEq-QewoE29N-P-3ult9qcwFHB&gclid=CjwKCAjwq7fABhB2EiwAwk-YbDghOZW1wSq0a1VFqOQJtPI8sVy8z8-Qd-qfAUh48uF_a-4DIRtH8hoCJ5sQAvD_BwE
- [70] Khan Academy, "Photoelectric Effect," Khan Academy. Accessed: Mar. 08, 2025. [Online]. Available: <https://www.khanacademy.org/science/modern-physics-essentials/x1bb01bdec712d446:why-light-and-matter-are-two-faced/x1bb01bdec712d446:einstein-s-elegant-equation-to-decode-the-photoelectric-effect/a/photoelectric-effect>

Appendix

Appendix A: Thesis Timeline – Gantt Charts

The Gantt charts presented below employ a colour-coded system to indicate the status of each task. Green cells denote completed tasks, yellow cells represent tasks currently in progress, and red cells indicate tasks that have been initiated but are not yet complete. Buffer periods are shaded in grey, as they are included as a precautionary measure and do not represent tasks requiring completion.

Appendix A.1: Term 1, 2025 Gantt Chart

Term 1, 2025											
Tasks	Time										
	February			March				April			
	W0	W1	W2	W3	W4	W5	W6	W7	W8	W9	W10
Laboratory Induction											
Equipment Operation Training											
Post Processing Training											
Ordering Components											
Preliminary Set up, Testing and Post Processing (Trial 1 Aligned 75 mm Roof)											
Literature Reading											
Literature Review											
Thesis A Report Drafting											
Thesis A Report Submission											

Figure 32: Term 1, 2025 Gantt Chart

Appendix A.2: Term 1-2 Break, 2025 Gantt Chart

Term 1-2 Break, 2025				
Tasks	Time			
	April	May		
	W1	W2	W3	W4
<u>SETUP, TESTING AND POST PROCESSING (ROOF)</u>				
Trial 1 Staggered 75 mm Roof				
Trial 1 Aligned 20 mm Roof				
Trial 1 Staggered 20 mm Roof				
Trial 1 Aligned 150 mm Roof				
Trial 1 Staggered 150 mm Roof				
Trial 2 Aligned 75 mm Roof				
Trial 2 Staggered 75 mm Roof				
Trial 2 Aligned 20 mm Roof				
Trial 2 Staggered 20 mm Roof				
Trial 2 Aligned 150 mm Roof				
Trial 2 Staggered 150 mm Roof				
Trial 3 Aligned 75 mm Roof				
Trial 3 Staggered 75 mm Roof				
Trial 3 Aligned 20 mm Roof				

Figure 33: Term 1-2 Break, 2025 Gantt Chart

Appendix A.3: Term 2, 2025 Gantt Chart

Term 2, 2025											
Tasks	Time										
	May	June				July				August	
	W0	W1	W2	W3	W4	W5	W6	W7	W8	W9	W10
<u>SETUP, TESTING AND POST PROCESSING (ROOF)</u>											
Trial 3 Staggered 20 mm Roof											
Trial 3 Aligned 150 mm Roof											
Trial 3 Staggered 150 mm Roof											
Trial 3 Aligned 75 mm Roof											
Trial 3 Staggered 75 mm Roof											
Buffer Period											
<u>SETUP, TESTING AND POST PROCESSING (PANEL)</u>											
Trial 1 Staggered 75 mm Panel											
Trial 1 Aligned 75 mm Panel											
Trial 1 Staggered 20 mm Panel											
Trial 1 Aligned 20 mm Panel											
Trial 1 Staggered 150 mm Panel											
Trial 1 Aligned 150 mm Panel											
Trial 2 Staggered 75 mm Panel											
Trial 2 Aligned 75 mm Panel											
Trial 2 Staggered 20 mm Panel											
Trial 2 Aligned 20 mm Panel											

Trial 2 Staggered 150 mm Panel											
Trial 2 Aligned 150 mm Panel											
Trial 3 Staggered 75 mm Panel											
Trial 3 Aligned 75 mm Panel											
Trial 3 Staggered 20 mm Panel											
<u>THESIS B REPORT</u>											
Thesis B Report Drafting											
Thesis B Report Submission											

Figure 34: Term 2, 2025 Gantt Chart

Appendix A.4: Term 3, 2025 Gantt Chart

Term 3, 2025											
Tasks	Time										
	September			October					November		
	W0	W1	W2	W3	W4	W5	W6	W7	W8	W9	W10
<u>SETUP, TESTING AND POST PROCESSING (PANEL)</u>											
Trial 3 Aligned 20 mm Panel											
Trial 3 Staggered 150 mm Panel											
Trial 3 Aligned 150 mm Panel											
Buffer Period											
<u>THESIS C REPORT AND PRESENTATION</u>											
Thesis C Report Drafting											
Thesis C Report Submission											
Thesis C Presentation Preparation											
Thesis C Presentation Submission											

Figure 35: Term 3, 2025 Gantt Chart

Appendix B: Evidence of Training on Specific Equipment

Appendix B.1: MME HSE Orientation session and Quiz

1/21/25, 3:56 PM

MME HSE Orientation session and Quiz

MME HSE Orientation session and Quiz

Points: 100/100

1. First Name *

Nathan



2. Family Name *

Sivalingam

3. ZID (place N/A if you don't know) *

z5359644

Figure 36: Evidence of MME HSE Orientation session and Quiz Completion.

Appendix B.2: Required Enrolment and Course Completion

2/9/25, 1:23 PM

Mail - Nathan Sivalingam - Outlook



Safety @ UNSW Complete

From (via UNSW) <noreply.moodle@unsw.edu.au>
Date Sun 09/02/2025 13:13
To Nathan Sivalingam <n.sivalingam@student.unsw.edu.au>

Congratulations on completing the UNSW Health and Safety Awareness training.

Your completion is registered in Moodle.

Note: This module covers the same content as:

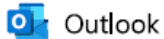
- HSEAWA & HSEEMT
- HSEAWC & HSEEMC
- HSECCA
- 'General Health & Safety Awareness' and 'Ergonomic Hazards and Manual Tasks'.

If there are any issues with demonstrating your completion to your Lab Manager or Supervisor, please show them this email or contact safetytraining@unsw.edu.au.

Figure 37: Evidence of *Safety@UNSW* Course Completion.

2/9/25, 1:41 PM

Mail - Nathan Sivalingam - Outlook



Lab Health and Safety Awareness training complete

From UNSW Safety (via UNSW) <noreply.moodle@unsw.edu.au>

Date Sun 09/02/2025 13:40

To Nathan Sivalingam <n.sivalingam@student.unsw.edu.au>

Congratulations on completing Lab Health & Safety Awareness training.

Your completion is registered in Moodle.

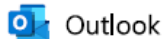
Note: This module covers the same content as HSELISO, HSELAB and Lab Health and Safety.

If there are any issues with demonstrating your completion to your Lab Manager or Supervisor, please show them this email or contact safetytraining@unsw.edu.au.

Figure 38: Evidence of *Lab Health & Safety* Course Completion

2/9/25, 2:04 PM

Mail - Nathan Sivalingam - Outlook



Hazardous Chemicals complete

From (via UNSW) <noreply.moodle@unsw.edu.au>

Date Sun 09/02/2025 14:04

To Nathan Sivalingam <n.sivalingam@student.unsw.edu.au>

Congratulations on completing both modules in the Hazardous Chemicals Safety training course.

Your completion is registered in Moodle.

Note: this course contains the same content as HSEHSO and 'Hazardous Chemicals Online'.

If there are any issues with demonstrating your completion to your Lab Manager or Supervisor, please show them this email or contact safetytraining@unsw.edu.au.

Figure 39: Evidence of *Hazardous Chemicals* Course Completion.

Appendix B.3: Induction into the Aerodynamics Lab



Approvals

Report • Printed on 26 April 2025

Approved

Induction Confirmation -Nathan Sivalingam-z5359644-J18 201/202 Aerodynamics Lab

Dear Nathan,

Please confirm that you have undertaken the induction to J18 201/202 Aerodynamics Lab and agree to abide by all the requirements outlined in the attached induction checklist by approving this request.

Your access will be activated within 48 hours after this approval is received.

Best Regards,
MME Technical Team

▼ Final status: Approved

NS

Approved by
Nathan Sivalingam

18/02/2025 10:27:38 am

MZ

Requested by
Mark Zhai

18/02/2025 10:27:07 am

Figure 40: Evidence of Aerodynamics Lab Induction.

Appendix C: Risk Assessment

Appendix C.1: Identify Hazards and Control the Risks

Table 7: Risk Assessment: Identify Hazards and Control the Risks.

Task/Scenario	Hazard	Associated harm	Existing Controls	Any additional controls	Risk Rating			Cost of controls (in terms of time, effort, money)	Is this reasonably practicable Y/N
					C	L	R		
Setting up the experimental rig.	Tripping over equipment both inside and outside the wind tunnel.	Slip/trip/fall injury	<ul style="list-style-type: none"> Ensure a clean workspace. Undergone extensive training in experimental setup. Enclosed shoes are always worn. Caution is taken when moving inside and outside the wind tunnel. 	No	2	C	M	Time, Effort	Y
	Jamming fingers in the experimental rig during the installation of the vortex generators.	Physical injury	<ul style="list-style-type: none"> Caution is taken when installing vortex generators onto the experimental rig. Two people should install the sections of the roof to reduce the chance of injury. 	No	2	C	M	Time, Effort	Y

	Touching the photovoltaic module when it is turned on.	Physical injury in the form of a burn.	<ul style="list-style-type: none"> Do not turn on the photovoltaic module until necessary to reduce the risk of accidental heat injuries. Practice extreme caution when the photovoltaic module is turned on. 	No	2	C	M	Time, Effort	Y
Turning the wind tunnel on and off.	Exposure to extremely high current can be fatal.	Physical injury/fatal	<ul style="list-style-type: none"> Follow the correct procedure outlined by Matthew Deng during the experimental testing demonstration. Press the emergency stop button located on the wind tunnel immediately if any problems are experienced. Do not attempt to fix any of the internal components of the wind tunnel under any circumstances. 	No	5	E	M	Time, Effort	Y
Operation of the wind tunnel.	Excessive noise caused by the wind tunnel.	Hearing loss	<ul style="list-style-type: none"> Use the ear plugs available in the lab during operation of the wind tunnel Once the wind tunnel is in operation, move 	No	2	D	L	Time, Effort, Money	Y

			to the enclosed room located at the end of the lab as it is generally quieter in there.						
General existence in the lab.	Potential exposure to chemical spills.	Slip/trip/fall injury	<ul style="list-style-type: none"> • Do not bring food and drink into the laboratory. • Exercise caution when walking through the laboratory. • If a spill has been identified as harmless, clean it up to avoid potential injury. • If the material is identified as harmful, alert the Lab Technical Officer immediately. 	No	2	C	M	Time, Effort	Y

Appendix C.2: Risk Rating Matrix

Table 8: Risk Assessment: Risk Rating Methodology and Matrix

RISK RATING METHODOLOGY AND MATRIX									
Consider the Consequences	Consider the Likelihood		Calculate the Risk						
Consider: What type of harm could occur (minor, serious, death)? Is there anything that will influence the severity (e.g. proximity to hazard, person involved in task etc.). How many people are exposed to the hazard? Could one failure lead to other failures? Could a small event escalate?	Consider: How often is the task done? Has an accident happened before (here or at another workplace)? How long are people exposed? How effective are the control measures? Does the environment affect it (e.g. lighting/temperature/pace)? What are people’s behaviours (e.g. stress, panic, deadlines) What people are exposed (e.g. disabled, young workers etc.)?		1. Take the consequences rating and select the correct column 2. Take the likelihood rating and select the correct row 3. Select the risk rating where the two ratings cross on the matrix below. VH = Very high, H = High, M = Medium, L = Low						
5. Severe: death or permanent disability to one or more persons 4. Major: hospital admission required 3. Moderate: medical treatment required 2. Minor: first aid required 1. Insignificant: injuries not requiring first aid	A. Almost certain: expected to occur in most circumstances B. Likely: will probably occur in most circumstances C. Possible: might occur occasionally D. Unlikely: could happen at some time E. Rare: may happen only in exceptional circumstances				Consequences				
					1	2	3	4	5
			Likelihood	A	M	H	H	VH	VH
				B	M	M	H	H	VH
				C	L	M	H	H	VH
				D	L	L	M	M	H
E	L	L	M	M	M				

Table 9: Risk Assessment: Risk Level and Required Action.

Risk Level	Required Action
Very High	<u>Act immediately:</u> The proposed task or process activity must not proceed. Steps must be taken to lower the risk level to as low as reasonably practicable using the hierarchy of risk controls
High	<u>Act today:</u> The proposed activity can only proceed, provided that: (i) The risk level has been reduced to as low as reasonably practicable using the hierarchy of risk controls and (ii) The risk controls must include those identified in legislation, Australian Standards, Codes of Practice etc. and (iii) The document has been reviewed and approved by the Supervisor and (iv) A Safe Working Procedure or Safe Work Method has been prepared and (v) The supervisor must review and document the effectiveness of the implemented risk controls
Medium	<u>Act this week:</u> The proposed task or process can proceed, provided that: (i) The risk level has been reduced to as low as reasonably practicable using the hierarchy of controls and (ii) The document has been reviewed and approved by the Supervisor and (iii) A Safe Working Procedure or Safe Work Method has been prepared.
Low	<u>Act this month:</u> Managed by local documented routine procedures which must include application of the hierarchy of controls.